Journal of Fluorescence, Vol. 4, No. 1, 1994

Laser-Induced Autofluorescence for Medical Diagnosis

K. Koenig[1,2] and H. Schneckenburger[1,3]

Received October 18, 1993

The naturally occurring autofluorescence of cells and tissues is based on biomolecules containing intrinsic fluorophores, such as porphyrins, the amino acids tryptophan and tyrosine, and the coenzymes NADH, NADPH, and flavins. Coenzymes fluoresce in the blue/green spectral region (fluorescence lifetimes: 0.5–6 ns) and are highly sensitive indicators of metabolic function. Steady-state and time-resolved blue-green autofluorescence is, therefore, an appropriate measure of the function of the respiratory chain as well as of cellular and tissue damage. Autofluorescence in the yellow/red spectral region is based mainly on endogenous porphyrins and metalloporphyrins, such as coproporphyrin, protoporphyrin (fluorescence lifetime of porphyrin monomers: >10 ns), and Zn-protoporphyrin (2 ns). Various pathological microorganisms such as *Propionibacterium acnes, Pseudomonas aeruginosa, Actinomyces odontolyticus, Bacteroides intermedius,* and *Saccharomyces cerevisiae* are able to synthesize large amounts of these fluorophores and can therefore be located. This permits fluorescence-based detection of a variety of diseases, including early-stage dental caries, dental plaque, acne vulgaris, otitis externa, and squamous cell carcinoma. The sensitivity of noninvasive autofluorescence diagnostics can be enhanced by time-gated fluorescence measurements using an appropriate time delay between ultrashort laser excitation and detection. For example, videocameras with ultrafast shutters, in the nanosecond region, can be used to create "caries images" of the teeth. Alternatively, autofluorescence can be enhanced by stimulating protoporphyrin biosynthesis with the exogenously administered porphyrin precursor 5-aminolevulinic acid (ALA). The fluorophore protoporphyrin IX (PP IX) is photolabile and photodynamically active. Irradiation of PP IX-containing tissue results in cytotoxic reactions which correlate with modifications in fluorescence due to photobleaching and singlet oxygen-dependent photoproduct formation. Therefore, on-line autofluorescence measurements during the phototreatment can yield information on the efficiency of ALA-based photodynamic therapy.

KEY WORDS: Autofluorescence; medical diagnosis; fluorophores; NADH; flavins; porphyrins; ALA.

INTRODUCTION

Ultraviolet (UV) and visible light exposure to cells and tissues results in the excitation of naturally occurring chromophores. Deactivation occurs in part via fluorescence emission. Intrinsic fluorophores with relatively high fluorescence quantum efficiencies are listed in Table I.

The amino acid trytophan is responsible for the UV fluorescence of most proteins [5]. The proteins collagen and elastin emit in the visible spectral region. Autofluorescence of the human skin is based partly on the excitation of these fluorophores. The reduced pyridine coenzymes nicotinamide adenine dinucleotide (NADH) and nicotinamide adenine dinucleotide phosphate (NADPH) fluoresce in the blue, while flavins emit in the green. The pyridine coenzymes as well as the flavin coenzymes act as sensitive indicators of metabolic function. The skin pigments melanin and bilirubin also ex-

[1] Institute of Lasertechnology in Medicine, Ulm, Germany.
[2] Beckman Laser Institute and Medical Clinic, Irvine, California.
[3] Fachhochschule Aalen, Department of Optoelectronics, Aalen, Germany.

1053-0509/94/0600-0017$07.00/0

Table I. Absorption and Fluorescence Maxima of Endogenous Fluorophores

Chromophore	Solvent	Absorption (nm)	Fluorescence (nm)
Tryptophan	H_2O	220,280,288	320–350 [1]
Thyrosin	H_2O	220,275	305 [2]
Collagen		300–340	420–460
Elastin		300–340	420–460
NADH	H_2O	260,340	470
NADPH	H_2O	260,340	470
Flavins	H_2O	260,370,450	530
Zn-coproporphyrin	DMSO	411,539,575	580
Zn-protoporphyrin	DMSO	421,548,585	592
Uroporphyrin	DMSO	404,501,533,568,622	624
Coproporphyrin	DMSO	398,497,531,565,620	622
Protoporphyrin	DMSO	406,505,540,575,630	633
Chlorophyll a	Ether	425,670	685 [3]
Chlorophyll b	Ether	455,642	660 [3,4]

hibit a fluorescence in the green with a maxima at 540 nm [6] and 520–540 nm [7], respectively, however their fluorescence quantum yields are very low (bilirubin, <0.001 [7]). Keratin, which can be found in the nails, emits at 525 nm [8]. Zn-porphyrins and metal-free porphyrins emit in the yellow/red spectral region. Some of them are precursors in heme biosynthesis. Chlorophyll can be found in plants and various bacteria and in intestine organs due to food uptake. In plants, chlorophyll fluorescence is a competitive process to the energy-transfer reaction in photosynthesis. Modifications to chlorophyll fluorescence may occur if reaction centers are closed or if the energy transfer from the antenna molecules is obstructed [9,10].

The detection of endogenous fluorophores by sensitive laser-induced autofluorescence yields information on the metabolic state, in particular in metabolism defects, and on the existence of various microorganisms. In addition, autofluorescence can be used to differentiate between various tissues.

This paper summarizes our efforts to develop medical applications of visible autofluorescence.

AUTOFLUORESCENCE DUE TO FLUORESCENT COENZYMES

The coenzymes NAD(H) and NADP(H), located mainly in the mitochondria of cells, act as hydrogen-transferring molecules in the respiratory chain (Fig. 1). The hydrogen uptake at position 4 of the pyridine ring results in significant spectral changes. These include the appearance of a new absorption band at 340 nm. Excitation of this electronic transition results in a fluorescence emission with a maximum at about 470 nm in aqueous solution. The reduced coenzymes possess a folded and an unfolded configuration [11,12]. The unfolded form, which is typical for bound coenzymes, shows a blue-shifted maximum.

The oxidized forms NAD and NADP fluoresce at about 445 nm. However, the fluorescence yield of the oxidized forms is 1000-fold less than the reduced forms (for excitation >300 nm). Therefore, in practice, UVA-excited *in vivo* fluorescence can be attributed to NADH/NADPH.

The spectra of oxidized flavomononucleotide (FMN), flavodinucleotide (FAD), and riboflavin are similar. They have main electronic transitions ($S_0 \rightarrow S_{1,2,3}$) at 260, 370, and 450 nm [13] and a fluorescence peak at 530 nm (Fig. 2). The FAD fluorescence quantum yield is a factor of 10 less than that of FMN and riboflavin [13]. Flavins possess a high intersystem crossing (ISC) rate. Deactivation of the triplet state occurs in part via phosphorescence at 605 nm [14]. Bound flavins, e.g., covalently attached to proteins (flavoproteins), show a bathochromic shift of the absorption bands to 280, 380, and 460 nm [13] and modifications to the emission spectrum.

Reduction of the isoalloxazine ring results in changes in the molecular configuration (planar into "butterfly" configuration), reduced absorption [13] and, consequently, decreased fluorescence. Most flavoproteins are only weak fluorophores.

The reduced pyridine coenzymes and the flavin/flavoprotein molecules have an emission bandwidth of about 80 nm and, therefore, overlap each other. Figure 3 demonstrates the emission spectrum of a coenzyme

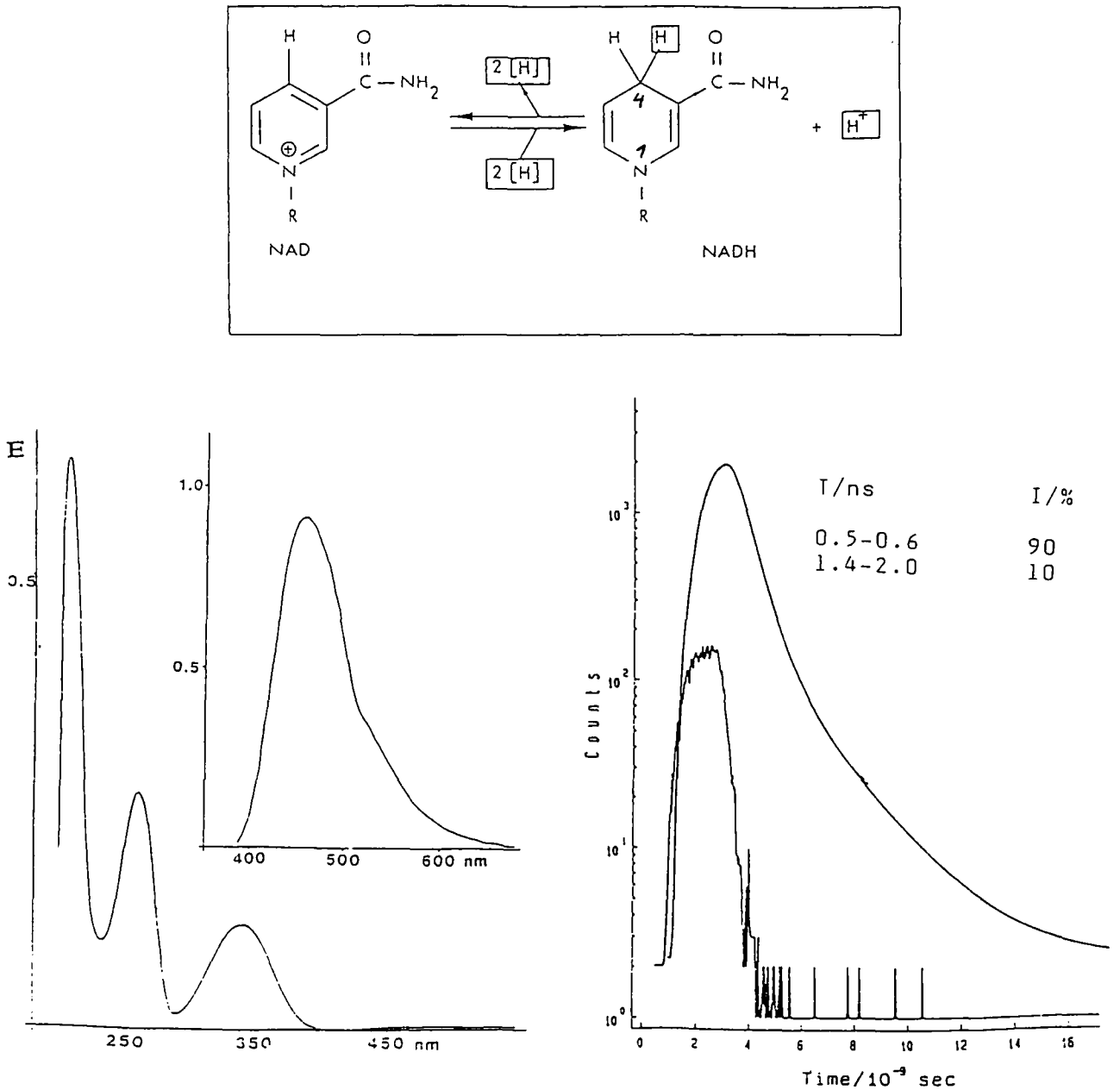

Fig. 1. Molecular structure, absorption and fluorescence spectra, and fluorescence decay kinetics of the pyridine coenzyme nicotinamide adenine dinucleotide. NADH, the reduced form of NAD, is formed by the hydrogen uptake at position 4 of the pyridine ring. NADH is reoxidized by transfer of electrons to a second acceptor. The 260-nm absorption band is due to adenine; the 340-nm band, due to the reduced pyridine ring. NAD possesses no 340-nm band.

mixture at different excitation wavelengths. Excitation at higher wavelengths results in a pronounced flavin emission. However, a clear differentiation of these coenzymes in cells and tissue is difficult. Another approach to separate these compounds is by time-resolved measurements. We determined the fluorescence decay kinetics of the coenzymes in aqueous solution by ultrashort laser excitation with a novel frequency-doubled laser diode at 390 nm (pulse duration, 40 ps) and the method of time-correlated single-photon counting (TCSPC) [16] (see Table III).

The free reduced pyridine coenzymes show in

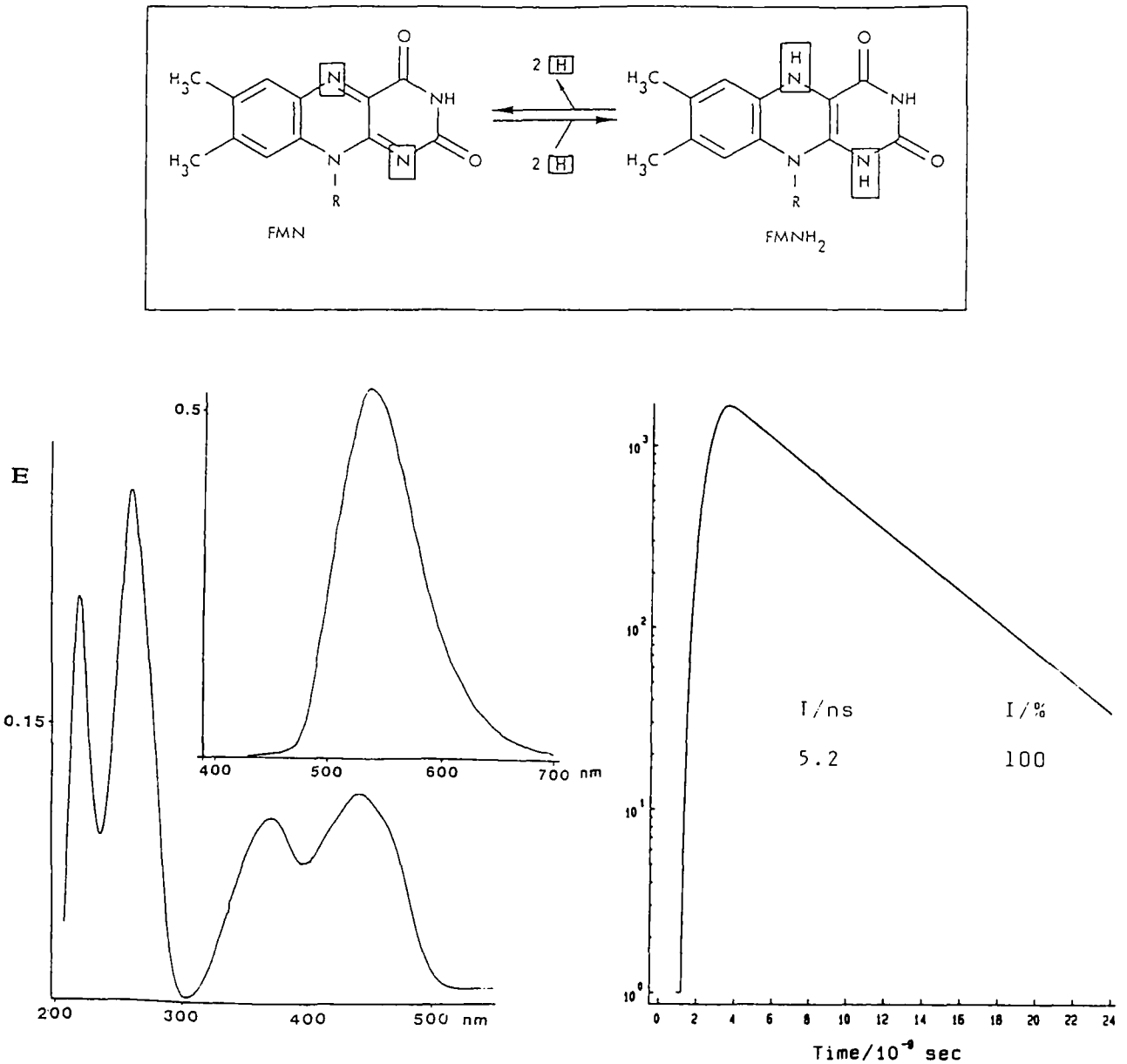

Fig. 2. Structure, absorption and fluorescence spectra, and fluorescence decay kinetics of FMN.

aqueous solution a biexponential behavior with a main fluorescence lifetime in the picosecond range, in contrast to monoexponentially decaying FMN, with a lifetime of about 5 ns. Bound NAD(P)M has a lifetime of 1-3 ns, whereas flavoflavins have picosecond lifetimes. A differentiation between type of coenzymes and free/bound status is therefore possible.

The fluorescent coenzymes act as sensitive bioindicators of metabolic functions such as the degradation of glucose or respiration. In particular, NADH may serve as an indicator of the intracellular oxygen concentration [17]. Any change in the oxygen supply results in changes in the mechanisms of electron transport of the respiratory chain. In particular, a reduced oxygen concentration leads to a higher NADH concentration. Therefore, the fluorescence of this reduced coenzyme enables the monitoring of the function of various intact organs. Already in 1959, Chance and Josis [18] studied the NADH emission during muscle contractions. Guezennec *et al.* [19] determined a NADH concentration of 0.087 mmol/kg in human muscle before, and a value of 0.184 mmol/kg at the moment of maximal contraction. They found that the corresponding fluoresence

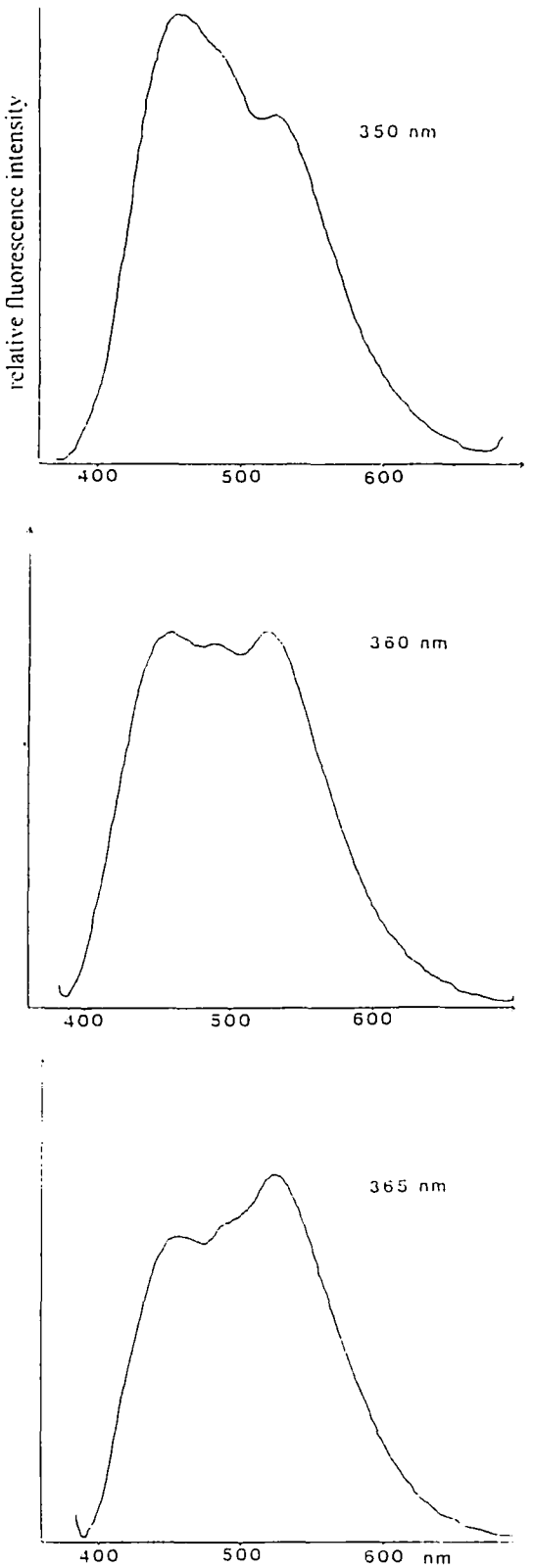

Fig. 3. Emission spectra of a mixture of NADH (10 μ*M*) and FMN (0.5 μ*M*) in aqueous solution [15].

increase occurred within 3 s. The increase in NADH concentration can be explained by local hypoxia and also by enhanced NADH synthesis due to higher activation of mitochondrial enzymes as a result of the calcium increase during muscle contraction [19].

The increase in NADH-induced fluorescence during ischemia, hypoxia, and anoxia was demonstrated by Mayevski [20] by *in vivo* fiber fluorometry on brain. These experiments show that it is possible to get on-line information on the oxygen status of organs by means of non- or low-invasive fluorescence detection.

Autofluorescence in the blue/green can also be used to differentiate between various tissues. Lohmann *et al.* [21,22] used the 365 nm-induced autofluorescence at 475 nm for tumor detection. They measured the autofluorescence of unstained cryosections of tumor- and surrounding tissue as well as the *in vivo* fluorescence of melanomas and found increased fluorescence intensity in the peritumoral regions. However, skin fluorescence in the blue/green spectral region is based on various fluorophores, such as collagen, elastin, and the coenzymes mentioned above. As a result, an exact determination of NADH emission is difficult. In the case of cryosections, the redox state of the coenzymes will be different from *in vivo* conditions.

We measured mitochondrial deficiencies in living cells by coenzyme-induced autofluorescence using video-enhanced/intensified microscopy and TCSPC. Different yeast strains (*Saccharomyces cerevisiae*) with genetic deficiencies of cytochromes *a*, a_3, and *b* in the respiratory chain and control strains [23,34] were used. Substructures of the cells with a diameter of about 5 μm were visualized by video-enhanced DIC (differential interference contrast) microscopy and combined with video-intensified fluorescence microscopy [16]. Excitation wavelengths at 365 and 436 nm were used for the pyridine coenzymes and the flavins, respectively. The corresponding cutoff wavelengths of the long-pass filters were 410 and 470 nm. It was found that the NADH-based autofluorescence of respiratory-deficient strains was a factor of 4 higher than that of intact strains (Fig. 4). Differences in flavin autofluorescence were less pronounced.

Cells showed a triexponential fluorescence decay pattern at 450 ± 20 and 500 ± 20 nm (excitation; 390 nm) (see Table II). The additional decay time and the differences compared to the measured values of free coenzymes can be explained by the existence of bound coenzymes (decay time of flavoproteins is mainly in the picosecond region [25]) and, in each case, by a small contribution of the other coenzyme. Differences between intact and defective strains occurred mainly in the lifetime and the relative intensity of the short-lived com-

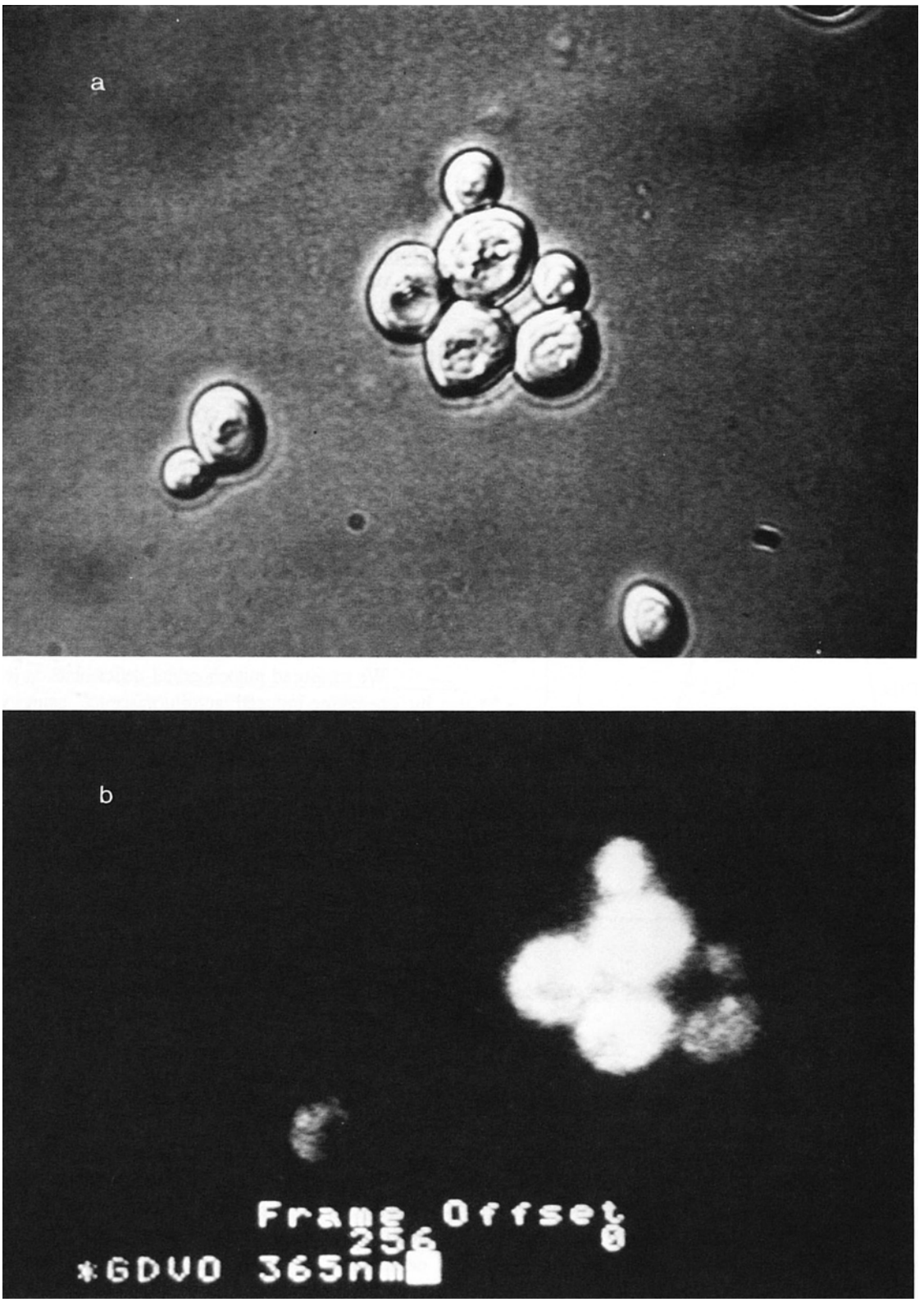

Fig. 4. DIC (a) and fluorescence images of respiratory-deficient (b) and intact (c) cells of *Saccharomyces cerevisiae*.

Fig. 4. Continued.

Table II. Fluorescence Lifetimes (T_i) and Relative Intensities (I_i) of Intact and Respiratory-Deficient Yeast Cells

Strain	λ (nm)	T_1 (ns)	I_1 (%)	T_2 (ns)	I_2 (%)	T_3 (ns)	I_3 (%)
Intact and defective	450	0.20–0.30	30	1.4–2.4	40	6.0–8.0	30
Intact	500	0.20–0.35	45	2.0–3.0	25	6.0–8.0	30
Defective	500	0.30–0.50	35	2.0–3.0	30	6.0–8.0	35

ponent detected at about 500 nm and are probably based on a different ratio of free-to-bound flavins. These results indicate that both, steady-state and time-resolved fluorescence can be used to probe the functioning of the respiratory chain.

In another study we investigated the modifications of autofluorescence during cell and tissue damage. The intracellular autofluorescence pattern of epithelial cells (RR 1022, Schmidt–Ruppin sarcoma), grown as monolayers on a slit, was measured using video-intensified microscopy. The cells were flooded with formalin. Simultaneously, the fluorescence was recorded (video frequency). A strong increase in intracellular fluorescence for 365-nm excitation (NADH/NADPH) and 405/436-nm excitation (flavins) was observed, indicating functional cell damage (Fig. 5). We measured a similar, but

less pronounced autofluorescence increase in the blue/green spectral region in the case of photodynamically induced cell damage [15]. Cell destruction was induced after incubation with the photosensitizer hematoporphyrin derivative (HPD), 5-aminolevulinic acid (ALA), or 8-methoxypsoralen (8-MOP) and light exposure [15,26]. Light activation of these agents results in phototoxic oxidation processes [27–29].

Similar autofluorescence measurements were carried out on live mice with subcutaneously transplanted G3 colon tumors. Six hours after intravenous ALA administration (280 mg/kg), the skin above the tumor was carefully removed. Then the tumor area was irradiated with 630-nm light (100 J/cm^2) from a dye laser. Autofluorescence was excited with the 351- or 407-nm line of a krypton ion laser. A shutter blocked the 630-nm radiation during fluorescence measurements. No significant fluorescence increase in the tumor or surrounding skin (fluorescence maxima, 460–475 nm for 351-nm excitation and 480–490 nm for 407-nm excitation) was measured during this photodynamic treatment; however, a strong increase occurred in the following 2 weeks [15]. This increased fluorescence was found to be located in limited areas of the irradiated tumor, probably indicating hypoxic or necrotic regions (Fig. 6).

Therefore, autofluorescence in the short-wavelength part of the visible spectrum can yield information on metabolic state, oxygen concentration, mitochondrial deficiencies, and tissue vitality.

PORPHYRIN-INDUCED AUTOFLUORESCENCE

Porphyrins are derivatives of the tetrapyrrole molecule porphin. They are the intermediate products in the synthesis of the metalloporphyrin heme [ferroprotoporphyrin (Fe^{2+})], hemin [ferriprotoporphyrin (Fe^{3+})], or chlorophyll, the latter containing magnesium as the central atom. All aerobic cells are able to synthesize hemeproteins [3]. The most important porphyrins in biological systems are the fluorophores protoporphyrin IX (PP IX), coproporphyrin III (CP III), uroporphyrin III (UP III), and hematoporphyrin IX (HP IX). In addition, UP I and CP I occur as by-products of the heme synthesis and are excreted in the urine and feces [3].

Normally, the concentration of porphyrins in biological tissue is extremely low. However, abnormalities in heme synthesis due to enzyme defects can cause a high accumulation of these metal-free fluorescent porphyrins. This results in strong red autofluorescence signals emanating from inner organs, erythrocytes, skin, urine, and feces. Corresponding diseases are termed porphyrias.

Two classes of hereditary porphyrias exist: (a) erythropoietic porphyria, where excessive amounts of UP, CP, or PP are accumulated in normoblasts and erythrocytes, and (b) hepatitic porphyrias [e.g., inherited porphyria cutanea tarda (PCT)], where an abnormal formation of heme precursors and Zn-porphyrins occurs in the liver [3]. Porphyrias are normally detected by determination of the porphyrin concentration in blood, urine, and feces by means of absorption or fluorescence measurements.

An abnormal accumulation of fluorescent porphyrins, mainly UP, CP, and PP, occurs also in some hemolytic diseases, anemia, and alcoholism. It can be induced by toxic chemicals such as chlorinated hydrocarbons or lead [3,30]. In the case of a decreased concentration of the enzyme uroporphyrinogen (UROD), the disease is termed chemical-induced or sporadic PCT. In particular, lead and ethanol activate the enzyme ALA-synthase and inhibit the enzyme ferrochelatase (responsible for the insertion of iron into PP) and, therefore, stimulate the porphyrin synthesis. Also, cases of estrogen-induced PCT [30] and PCT of patients with HIV-1 infection [31] have been reported.

In addition to enzyme defects, various microorganisms can provide endogenous porphyrins. For example, certain species of the genus *Bacteroides* produce PP. These anaerobic bacteria belong to the normal flora of the oral cavity and intestine [32]. Also, the skin bacterium *Propinibacterium acnes* emits in the red spectral region [33–35], as do some strains of *Clostridium, Bifidobacterium, Actinomyces* [36], *Bacillus thuringiensis* [37], and *Staphylococcus aureus* [38].

Some microorganisms contain chlorophyll. These photosynthetic microbiological cells fluoresce in the far-red spectral region. Interestingly, fluorescence in this region can sometimes be found in the skin, urine, feces, stomach, and intesine [39–41]. This emission is typically caused by food. For example, cereal corns emit at about 677 nm [41]. The responsible fluorophores are chlorophyll or photodegradation products of chlorophyll, such as pheophytin or pheophorbide [40]. These reduced porphyrins can be formed by a photoinduced demetallation process and by phytol chain removal [42].

The absorption spectrum of metal-free porphyrins consists of a major band at about 400 nm, the so-called Soret band, and four smaller Q-bands in the longer-wavelength part of the visible spectrum (Fig. 7). With the exception of UP, porphyrins aggregate in aqueous solution and deaggregate in ethanol or in the presence of serum albumin. Dimers and higher aggregates show

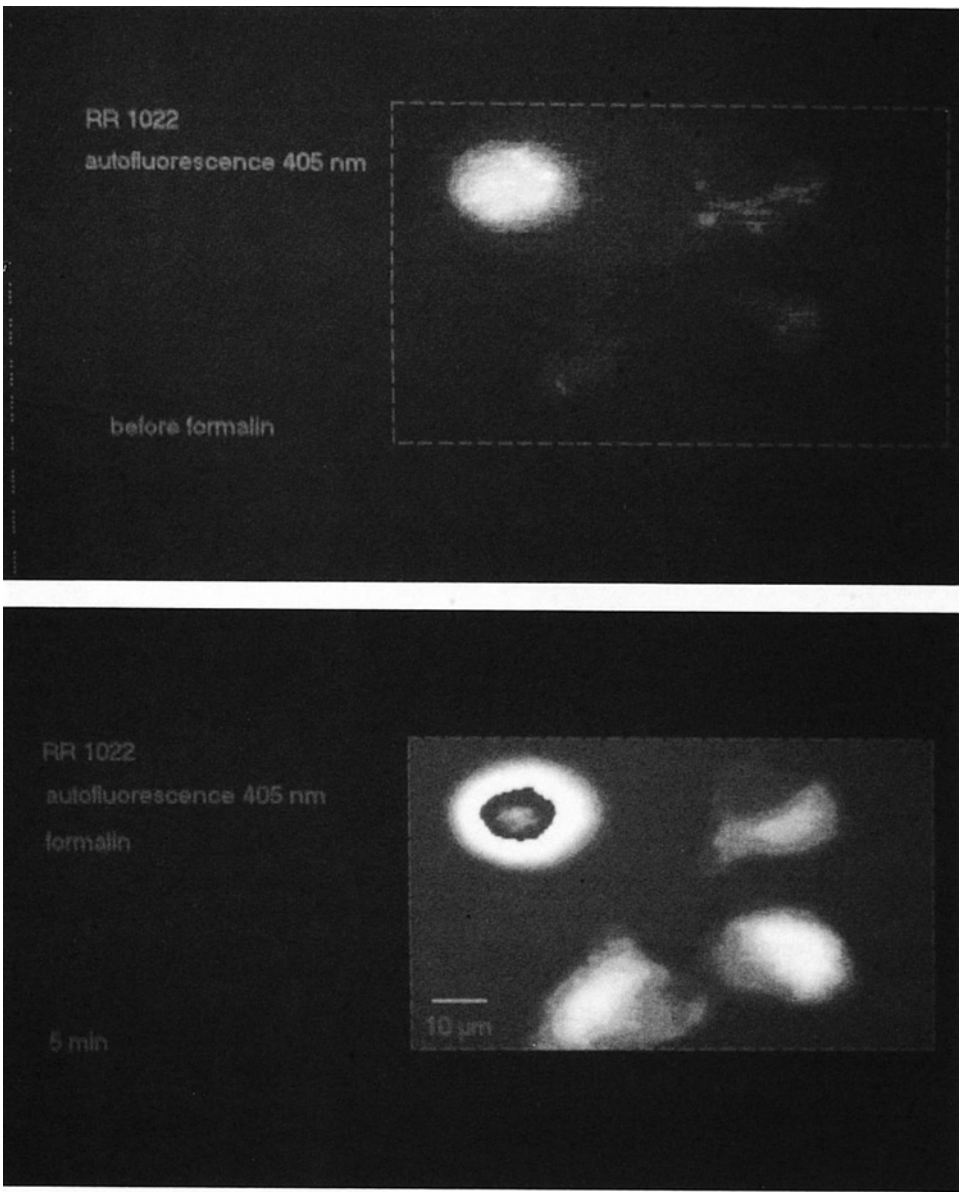

Fig. 5. Micrographs of the intracellular autofluorescence in the blue/green spectral region of epithelial cells before and during incubation with formalin.

a blue shift of the Soret band and have a lower fluorescence quantum efficiency than monomers. Therefore, the optimal fluorescence excitation wavelength should be about 400 nm. Appropriate excitation sources are the mercury lamp, with a strong emission at 405 nm, and the krypton ion laser, at 407 nm. However, this excitation radiation is also absorbed by the non-fluorescent hemoglobin. This competitive absorber limits the penetration depth of the excitation radiation to be in the micrometer range. To get information on deep-lying porphyrins, longer excitation wavelengths corresponding to the Q-absorption bands can be chosen [41].

TUMOR DIAGNOSIS DUE TO FLUORESCENT ENDOGENOUS PORPHYRINS

There is a great probability that mutagenic cells show enzyme defects which can result in a preferential

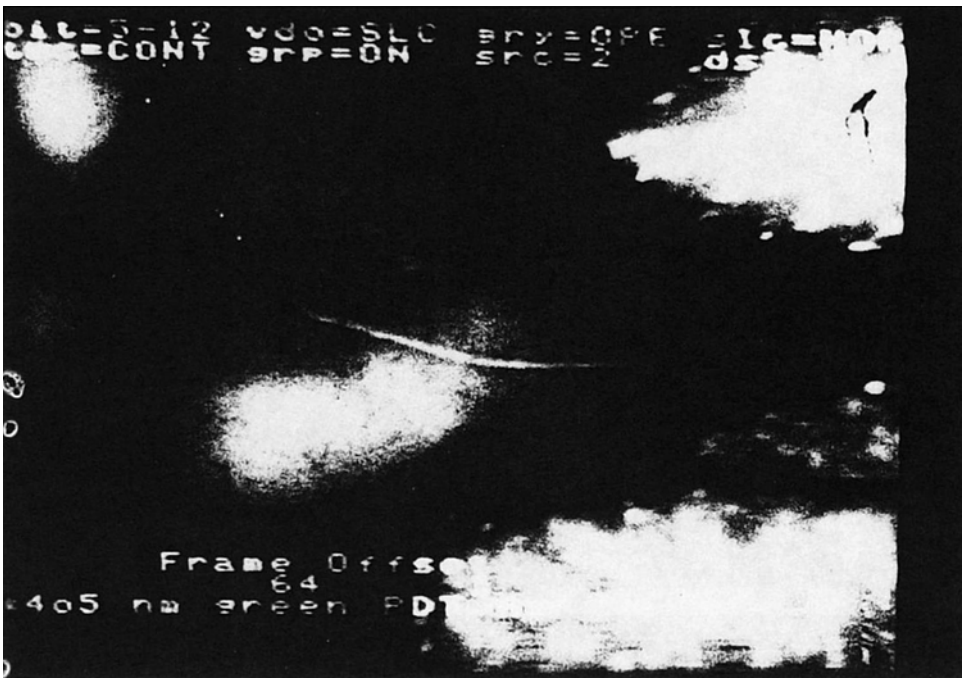

Fig. 6. Micrographs (2.5×) of *in vivo* tumor and skin autofluorescence 7 days after ALA phototreatment (λ_{exc} = 436 nm, λ_F = 470–570 nm). Fluorescent sites on the right: skin emission; in the middle: tumor emission.

porphyrin accumulation. Indeed, as early as 1924 Policard [43] observed a red autofluorescence in tumors during excitation with a Wood's lamp and suggested HP as the responsible fluorophore. This UV lamp is named after Wood, who developed short-pass liquid (nitrodimethylanilin) and glass filters for absorbing visible light, thus leading to the construction of "pure" UV sources [44]. Gougerot and Patte [45], in 1939, Rochese [46], in 1954, and Sharvill [47], in 1955, noted similar fluorescence using this UV lamp. In 1960, Ghadially [48,49] reported that endogenous PP IX is the main fluorophore responsible for red autofluorescence in chemically induced animal tumors. Three years later, he and his coworkers [50] suggested that microbial synthesis is the origin of the porphyrin accumulation in tumors. Harris and Werkhaven [51] visualized the red emission of oral cancers by means of a fluorescence lamp as an excitation source and viewing through laser-guard argon goggles. Alfano *et al.* [8] excited tissue samples with the 488-nm line of an argon ion laser and found peaks between 590 and 600 nm in tumor tissue. Yuanlong *et al.* [52] measured biopsies of squamous cell carcinoma 4 h after removal and found 89% agreement between red autofluorescence and the traditional biopsy method. The 365-nm line of a pulsed xenon ion laser served as the excitation radiation. They suggested that autofluorescence is based on the accumulation of certain degradation products of hemoglobin in cancer tissue.

We measured autofluorescence *in vivo* using the 364-nm line of an argon ion laser and a fiber-optical sensor and found strong signals at 673 nm in the skin, at 638 and 680 nm in subcutaneously transplanted solid Ehrlich carcinoma of mice [39], and at 635 nm in patients with squamous cell carcinoma [40]. The sensitivity of the measurements could be enhanced by using the 407-nm radiation of a krypton ion laser and a sensitive detection system consisting of a fiber-optic sensor, polychromator, and multichannel analyzer (Fig. 8).

Biopsies of 30 oral human squamous cell carcinomas were measured 1 h after removal [53]. The biopsies were stored in 0.9% NaCl. Only 20% of the biopsies showed a weak autofluorescence in the red spectral region. These samples showed necrotic regions. No fluorescence was found in biopsies from surrounding sound tissue. The autofluorescence spectrum of the carcinoma consisted of a major peak at 636 nm, typical of PP. Five biopsies showed an additional peak in the 580- to 600-nm region (Fig. 9a) where Zn-PP emits. All fluorescent biopsies were stored in glass vials at room temperature

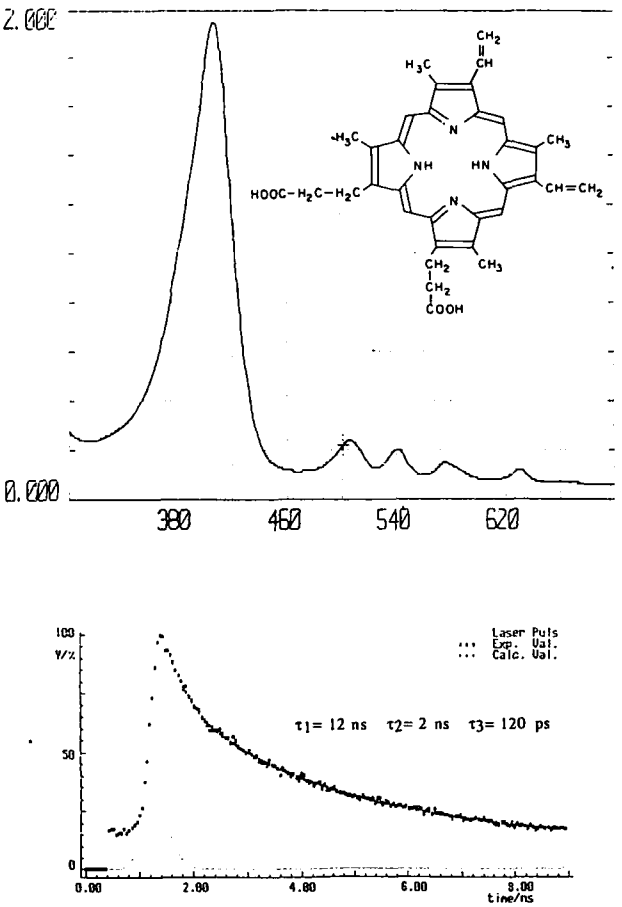

Fig. 7. Top: Structure and absorption spectrum of PP IX in DMSO. Bottom: Typical fluorescence decay curve of metal-free porphyrins in aqueous solution with decay times at 12 ns (monomers), 2 ns (dimers), and 100 ps (higher aggregates).

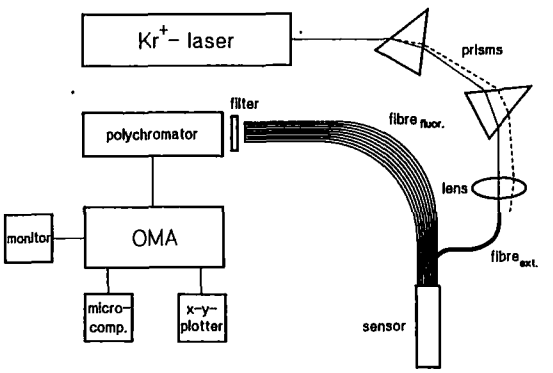

Fig. 8. *In vivo* fluorescence spectrometer.

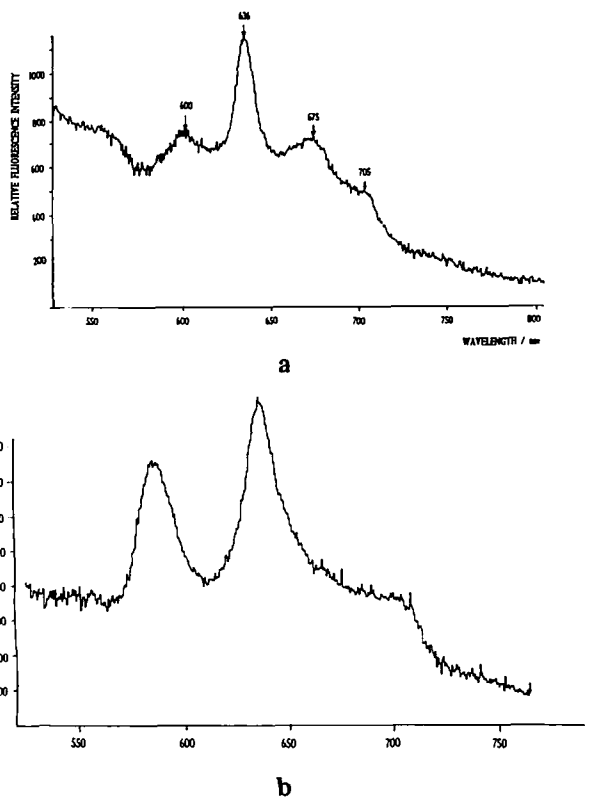

Fig. 9. (a) Autofluorescence spectrum of an oral squamous cell carcinoma, 1 h after removal. Peritumoral tissue showed no porphyrin fluorescence. (b) Autofluorescence 2 weeks later.

and showed a significant increase in fluorescence over the following 2 weeks (Fig. 9b). The band at 580 nm became the new spectral maximum, probably due to the insertion of zinc into endogenous PP. Metallation was also observed for free porphyrins stored in glass vials (glassware contains zinc) [54–56].

In another study we divided a freshly removed weak-fluorescent biopsy into three parts. One was stored in NaCl solution, the second in formalin, and the third in NaCl solution incubated with antibiotics (Polymexin E). Only the first developed strong autofluorescence in the red spectral range. The increase in fluorescence in NaCl-stored biopsies can be explained by microbial synthesis of PP. When samples were assayed for bacteria, the fluorescent *Pseudomonas aeruginosa* was isolated (Fig. 10). Our results confirm that the red autofluorescence which can be found in some oral squamous cell carcinomas originates from fluorescent bacteria, and not from enzymatic defects in heme synthesis. High concentrations of these bacteria can be found in necrotic and ulcerated tumor tissues. Thus, red autofluorescence does not seem to be an appropriate method for the detection of early-stage squamous cell carcinoma.

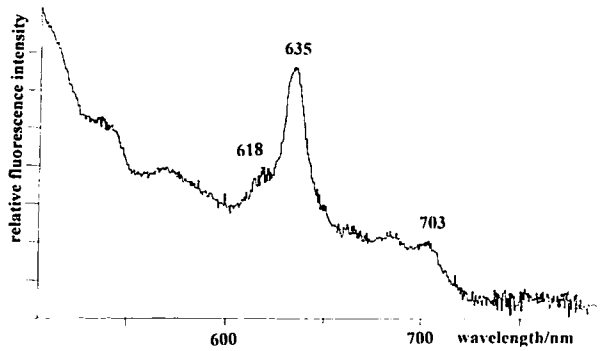

Fig. 10. Autofluorescence spectrum of the Gram-negative bacterium *Pseudomonas aeruginosa.*

Many efforts have been made to employ autofluorescence for tumor detection. Some studies have concentrated on emission in the short-wavelength part of the visible spectrum [21,22,57–60]. As mentioned before, Lohmann *et al.* [21,22] measured UV-excited emission at 475 nm. Montan and Stroemblad [57] found tumor-specific emission bands at 390 and 435 nm. Alfano *et al.* [8] measured a tumor-specific peak at 521 nm when excited with 488-nm radiation. Hung *et al.* [58] found differences in fluorescence intensity only between tumor and peritumoral tissue. Tang and Alfano [59] explained the spectral differences between normal and cancerous tissues by the influence of different hemoglobin absorption.

Despite promising preliminary results, further investigations are necessary before laser-induced autofluorescence can be used clinically for the diagnosis of early-stage cancer.

IN VIVO DETECTION OF BACTERIA IN HUMAN SKIN

The Gram-positive bacterium *Propionibacterium acnes* belongs to the normal flora of human skin. It is involved in the pathogenesis of the widespread skin disease acne vulgaris. This bacterium synthesizes CP and PP [33–35,61–64]. The significance and the optimal conditions for the porphyrin synthesis are not well studied. These endogenous porphyrins are responsible for the yellow/red autofluorescence of human skin. As early as 1927, Bommer [44] reported orange skin fluorescence when irradiated with the Wood lamp.

We carried out fluorescence imaging and spectral analysis of different skin areas (face, back) of 30 test patients with and without acne vulgaris [65]. For that purpose we used the *in vivo* fluorescence spectrometer depicted in Fig. 8 and a color CCD camera combined with a long-pass filter (cutoff wavelength, 550 nm). All persons excited with the 407-nm radiation of the krypton ion laser showed strong fluorescent spots in the skin, mainly in the nasal region and in pimples of acne patients (Fig. 11). These spots localize sebaceous follicles which contain large amounts of *P. acnes.* The spots differ in color; most fluoresce in the yellow or red. Their spectrum consists of three main peaks, at about 580–600, 620, and ~640 nm, as shown by the spectral analysis of single fluorescent spots (diameter of the excitation fiber, 0.2 or 0.6 mm) (Fig. 12). The primary peak was at 600 nm, indicating the existence of metalloporphyrins, probably Zn-PP.

Extracted sebaceous follicles showed spectra similar to the *in vivo* skin spectrum. We isolated *P. acnes* from these follicles. The spectral behavior of the bacteria grown on agar (blood agar base No. 2; OXOID) under dark conditions at 37°C in anaerobic jars (Gas Pack System; OXOID) was different. We found bacterial colonies with either a 635-nm fluorescence band (PP) or a 620-nm band (CP) or colonies which emit both bands. No metalloporphyrin peak was found. The incorporation of zinc may therefore occur in the skin by the uptake of dermal zinc. We varied the pH value of the agar medium to study the pH influence on the spectral behavior but found no dependence of the ratio of the fluorescence intensities at 635 to 620 nm.

In situ autofluorescence imaging of the human skin is a rapid detection method which can be used to localize fluorescent bacteria. It is of special interest for the diagnosis of acne and seborrhoic diseases and allows the rapid noninvasive control of treatments, especially in the case of antibiotic therapy and UV phototreatment [66,67].

DIAGNOSIS OF CARIES AND DENTAL PLAQUE

In 1927 Bommer investigated his patients with the Wood lamp and found an orange and red fluorescence of the tooth film [44]. Benedict [68] and Hartles and Leaver [69] reported on tooth fluorescence under UV irradiation. Armstrong [70], in 1963, studied the fluorescence of healthy and carious human dentine preparations. Since the eighties, different groups [71–76] have tried to localize carious regions by means of laser-induced autofluorescence. Alfano *et al.* [74] measured a fluorescence maximum at 550 nm in carious lesions when excited with 488-nm radiation. Albin *et al.* [75] found an emission peak at 590 nm in dental caries.

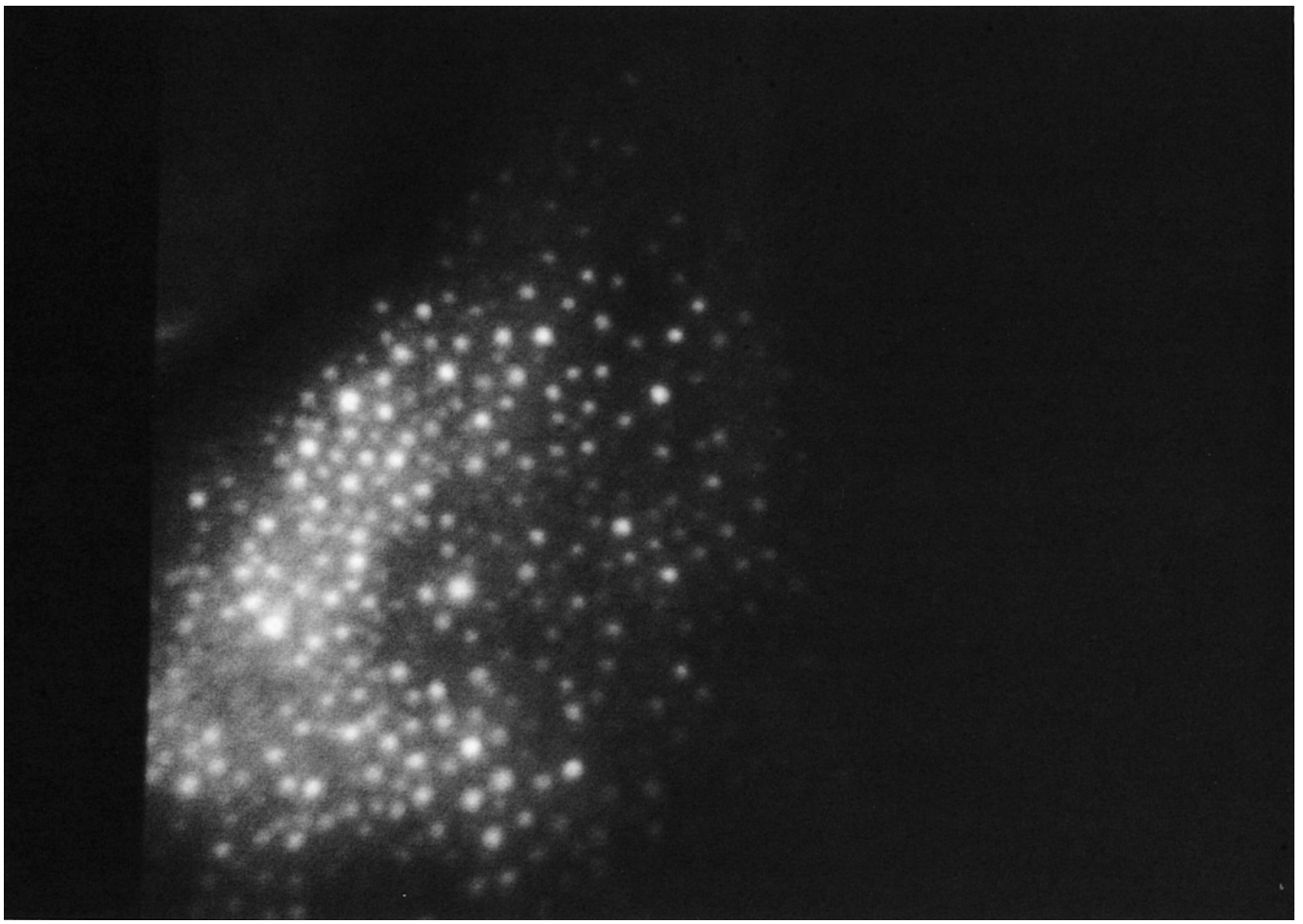

Fig. 11. Autofluorescence spectrum of the author's nose (kk). The fluorescent spots localize sebaceous follicles which contain large amounts of porphyrin-producing *Propionibacterium acnes.*

We investigated the autofluorescence of about 100 freshly extracted human teeth using violet excitation, the optimal excitation source for porphyrins [77,78]. It was found that healthy dental tissue (enamel, dentin) showed a broad emission band in the short-wavelength part of the visible spectrum. In contrast, the fluorescence spectrum of all carious lesions consisted of maxima in the red spectral region, with a main band at 635 nm. A clear differentiation between healthy and carious tissue was possible. Less than 10% of the teeth showed an additional band at about 590 nm and shoulders at 620 nm (Fig. 13). *In vivo* measurements on patients, using a single detection fiber, showed similar spectra in regions of dental caries.

As mentioned, the maxima at 635, 620, and 590 nm correspond to the emission peaks of PP, CP, and Zn-PP in hydrophobic environments. HPLC measurements confirm the existence of these chromophores in a concentration range of several picomoles per milligram dry weight in the carious lesion [78]. The question arises regarding the origin of these endogenous porphyrins in dental caries. We investigated various cell cultures which can be found in caries and dental plaque. Hardie and Bowden [79] found that the bacteria *Streptococcus, Actinomyces*, and *Bacteroides* are the microorganisms mainly responsible for the plaque flora.

No porphyrin fluorescence in the red spectral region was measured for the bacterial strains *Streptococcus mutans* and various *Lactobacteria* grown on agar plates. However, a strong fluorescence with maxima at 635 and 700 nm was detected in the bacterial strains *Actinomyces odontolyticus, Bacteroides intermedius* (strongest fluo-

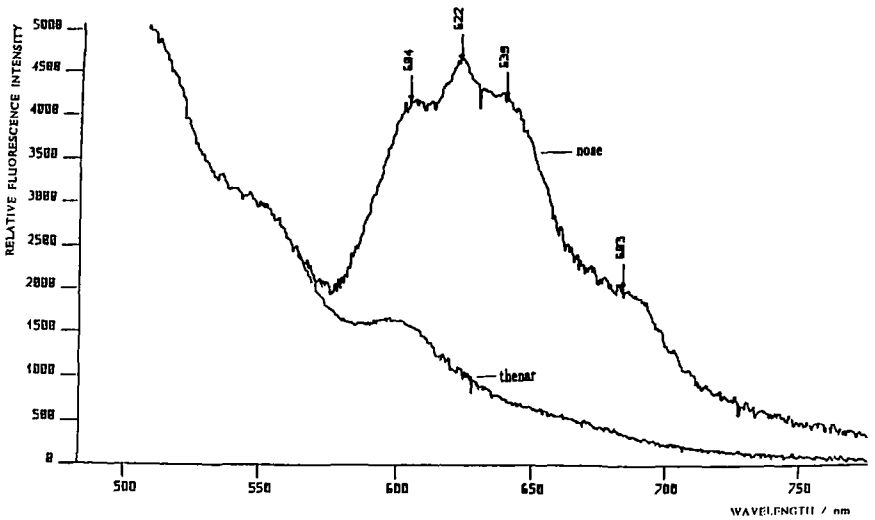

Fig. 12. *In vivo* autofluorescence spectrum of a fluorescent spot in the human skin. The spectrum is a superposition of the fluorescence of PP, CP, and probably Zn-PP.

rescence) (Fig. 14), and *Pseudomonas aeruginosa.* The microorganism *Candida albicans* and *Corynebacterium* emitted at about 620 nm (CP).

Our results demonstrate that the red autofluorescence characteristic of caries and dental plaque is based on porphyrin-synthesizing oral bacteria present in dental lesions. One problem of early-stage caries diagnosis by autofluorescence is the emission of the surrounding healthy tissue. As shown, this fluorescence shows no structured spectrum in the red spectral region. However, the fluorescence intensity at 635 nm of the healthy tissue can be higher than the caries peak in the case of very small lesions or early-stage caries. One solution to this problem is the use of time-gated fluorescence technology as demonstrated below.

ENHANCEMENT OF AUTOFLUORESCENCE

The autofluorescence of cells and tissues can be enhanced by stimulated biosynthesis of endogenous fluorophores. For example, the production of endogenous porphyrins can be stimulated by the modification of enzyme activity, the application of iron scavengers, or the external administration of porphyrin precursors. Figure 15 demonstrates the schematic pathway of heme synthesis. Each nucleated mammalian cell is able to synthesize heme-containing enzymes. Catalytic reactions lead to the formation of the precursor ALA due to the ALA synthase-catalyzed condensation of glycine with succinyl-CoA (C_4 pathway, mammalian cells) or due to a C_5 pathway from L-glutamate (some bacteria, algae, plants) [80]. In the next step, the enzyme ALA dehydratase catalyzes the formation of porphobilinogen from two ALA molecules. Further reactions lead to the synthesis of PP IX, followed by the ferrochelatase-catalyzed iron insertion process that results in heme. Heme provides negative feedback on the activity of the enzyme ALA synthase (located in the mitochondrial matrix) and therefore limits the synthesis intracellular ALA [81].

However, external administration of ALA bypasses normal heme regulation. This results in increased synthesis of PP and heme and an increase in autofluorescence. The efficiency of the PP IX synthesis depends on the kind of cell. For example, less synthesis occurs in the dermis compared with the epidermis. Endometrium produces a higher amount of PP than myometrium [82]. Rapidly dividing tumor cells accumulate more PP than normal cells as shown, e.g., by Malik and Djaldetti [83] in the case of leukemia cells or by Baumgaertner *et al.* [84] after ALA instillation in the bladder.

Kennedy and Pottier [28] have used ALA-induced formation of PP in cancer research. They applied topical ALA to various skin tumors and obtained selective accumulation in tumor tissues. Selectivity can be explained by the absence of penetration through the intact stratum corneum of the surrounding healthy skin, in contrast to the defective keratin layer common to skin abnormalities such as tumors and psoriasis.

PP synthesis in well-defined skin areas can be ob-

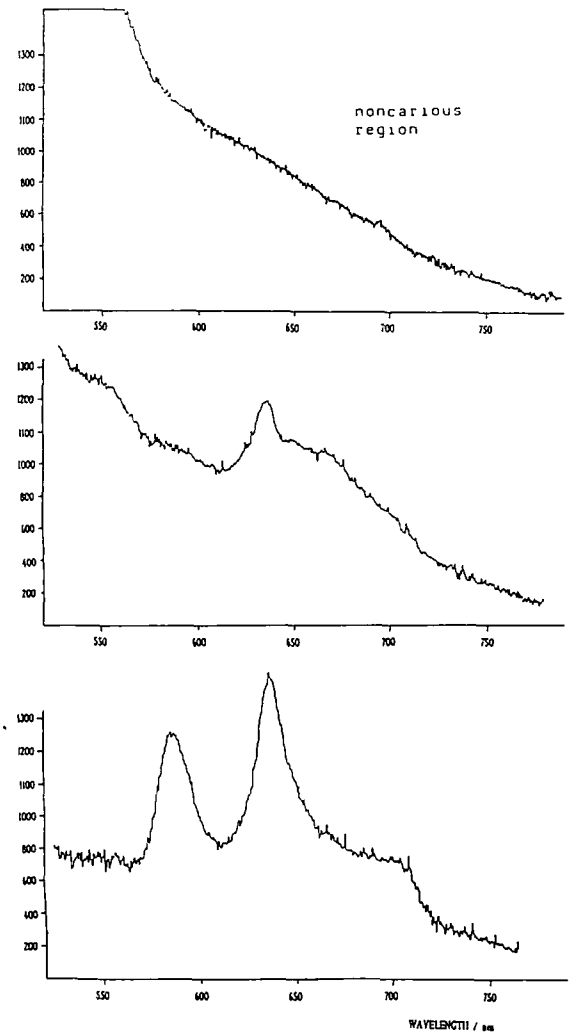

Fig. 13. Autofluorescence spectra of various regions of freshly extracted human teeth with carious lesions.

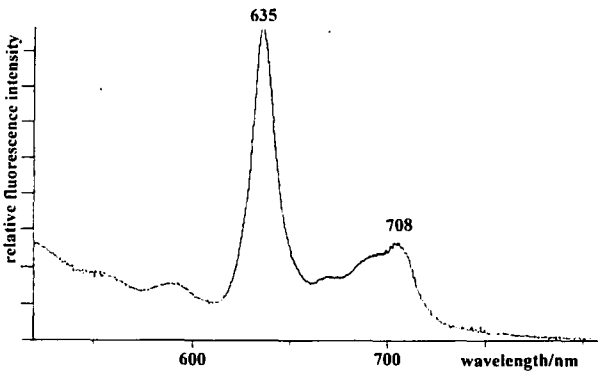

Fig. 14. Autofluorescence of the Gram-negative bacterium *Bacteroides intermedius* on agar plates containing blood. These bacteria are able to remove iron from blood (demetallation process).

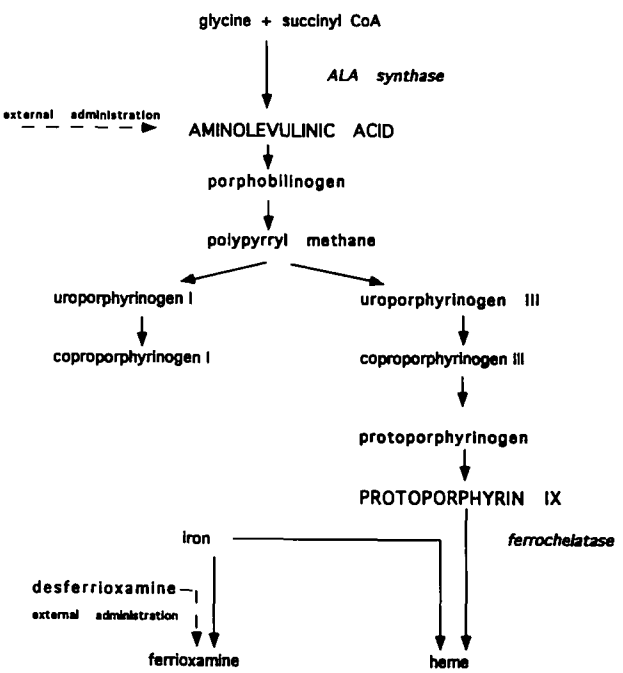

Fig. 15. Schematic pathway of heme biosynthesis. External administration of ALA bypasses the heme regulation (negative feedback) and leads to enhanced PP IX production. A further increase in PP IX concentration can be achieved by the additional application of desferrioxamine. One mole of this agent binds 1 mole of iron, forming the stable iron complex ferrioxamine.

tained after removal of the stratum corneum and topical ALA administration. We removed this layer by ablation using an Er:YAG laser and found the PP IX fluorescence only in the region of tissue ablation [85]. The maximum of the fluorescence occurred 4–6 h after ALA administration and dropped to 37% (1/*e*) within 12 h.

The PP content in cells and tissues can also be enhanced by the administration of agents with a high affinity for iron, such as desferrioxamine. This results in a reduced rate of iron insertion in PP molecules and therefore in a reduced rate of heme synthesis. In addition, more intracellular ALA is produced due to diminished feedback regulation (see Fig. 15).

Figure 16 shows our results of tumor fluorescence after ALA and desferrioxamine administration. The fluorescence signals at 635 nm of two groups of xenotransplanted G2 bladder tumors were compared: One group was incubated with ALA alone (280 mg/kg, i.v.); the other, with ALA and desferrioxamine (0.75 mg, intratumoral). A faster fluorescence rise and higher intensity

were found in the case of simultaneous ALA and desferrioxamine administration [86].

As mentioned before, another way to increase porphyrin accumulation is the modification of the enzyme activity. It has been shown by several groups that exposure of cells to chemical substances, such as DDC, EDDC, and griseofulvin, results in inhibition of ferrochelatase [87–89]. Malik *et al.* [90] found that when melanoma cells were exposed to ALA in the presence of DMSO and allylisopropylacetamide, PP IX levels increased from 8 to 22,000 pmol/mg cell protein. Javor and Febre [91] stimulated porphyrin synthesis in *Escherichia coli* by application of 1-thioglycerol. The autofluorescence in microorganisms can also be enhanced by the external administration of ALA [92,93]. However, bacteria from the genus *Bacteroides* show another pathway of PP accumulation. They are able to remove iron from heme or blood and fluoresce due to this demetallation process [32].

In conclusion, the stimulation of the biosynthesis of metal-free porphyrins in microorganisms and tissues enhances autofluorescence and can be used for detection of microorganisms and diseases, in particular for cancer diagnosis.

ENHANCEMENT OF THE SENSITIVITY OF AUTOFLUORESCENCE DIAGNOSTICS BY TIME-GATED FLUORESCENCE MEASUREMENTS

The sensitivity of noninvasive autofluorescence diagnostics can be enhanced by time-gated fluorescence measurements using an appropriate ultrashort time interval of detection. The idea is to consider the different fluorescence decay kinetics of the various endogenous fluorophores and to choose an appropriate time window which isolates the compound of interest. In addition, scattered excitation light can be excluded with sufficient time delay between ultrashort laser excitation and detection. A preferential application of this method is the detection of metal-free porphyrin monomers. These fluorophores have fluorescence decay times greater than 10 ns. Other endogenous chromophores possess shorter fluorescence lifetimes (see Table III). PP, CP, and HP aggregate in aqueous solution, resulting in a blue shift of the Soret band and an additional fluorescence peak at about 650–670 nm. Dimers have a fluorescence lifetime of about 2 ns; higher aggregates of about 100 ps [94–96].

We found that ALA-induced PP in cells showed a nearly monoexponential fluorescence decay [97] and conclude, therefore, that intracellular formed PP exists mainly in its monomeric form (Fig. 17). The fluorescence decay curves in tissue are more complicated. Because of multiple scattering, fluorescent photons can be distributed along various paths, leading to an additional time delay for photons arriving at the detector. Although this effect may artificially extend decay curves, we expect that for 390-nm excitation, only superficial fluorophores will be excited and lifetime errors will occur in the picosecond range only. Figure 18 demonstrates the decay pattern of normal and ALA-stimulated autofluorescence of human skin. It is obvious that skin incubated with ALA contains a long-lived fluorophore which can be attributed to PP monomers. It should therefore be possible to detect porphyrin monomers very sensitively by choosing a time delay of more than 10 ns between excitation and detection.

Figure 19 shows the experimental setup for time-gated imaging and time-gated spectroscopy in the nanosecond region. It consists of a fluorescence microscope with a highly sensitive videocamera (Proxitronic, NCA)

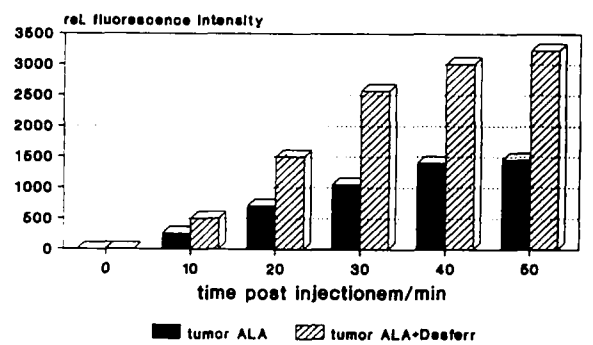

Fig. 16. *In vivo* autofluorescence of a xenotransplanted G2 bladder tumor after administration of ALA alone and in combination with desferrioxamine (Desferr).

Table III. Fluorescence Decay Times of Fluorophores

Fluorophore	Solvent	T_1 (ns)	I_1 (%)	T_2 (ns)	I_2 (%)
NAD(P)H	H_2O	0.45–0.60	75–90	1.4–2.2	10–25
FMN	H_2O	5.2	100		
Flavoproteins	H_2O	<1			
Collagen	powder	2.7	25	8.9	35
Elastin	powder	2.0	75	6.7	65
Zn-PP	DMSO	2	100		
PP IX	DMSO	17	89	3	11
CP IX	DMSO	20	100		
PP photoproducts	DMSO	0.7	38	4.5	62

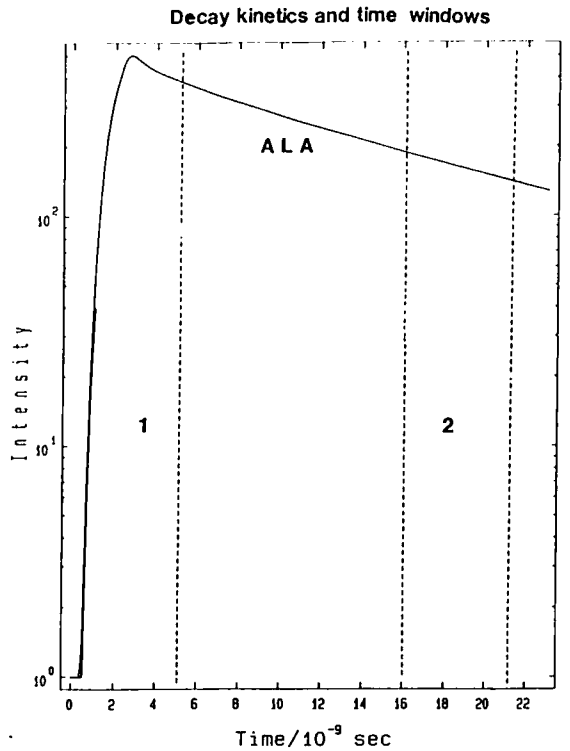

Fig. 17. Fluorescence decay kinetics of an ALA-incubated chorioallontoic membrane (CAM) of a chicken embryo.

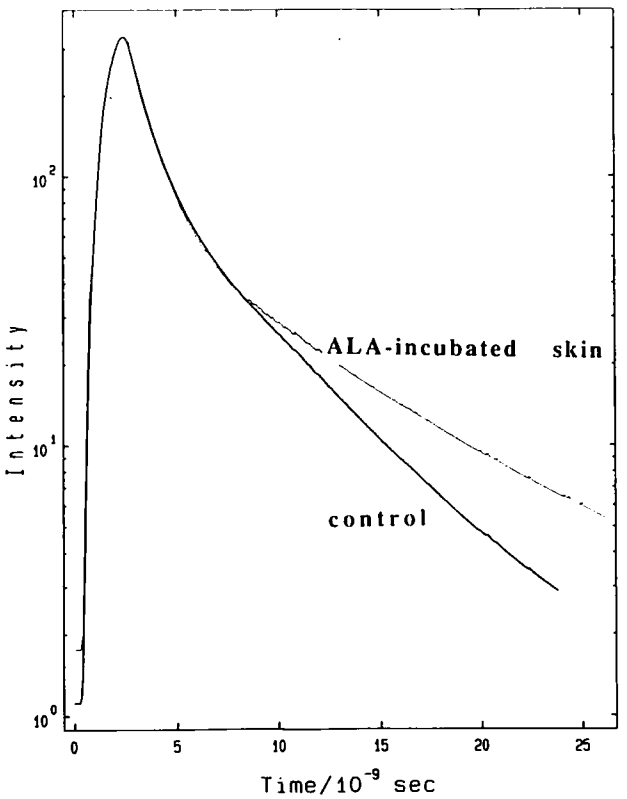

Fig. 18. Fluorescence decay pattern of skin after laser removal of stratum corneum and topical ALA administration. The detection area was greater than the ALA-treated area. Therefore, superimposition of normal autofluorescence and PP IX fluorescence occurs.

and a monochromator combined with an optical multichannel analyzer (Hamamatsu, IMD, C4562). The image intensifiers of both detectors are time-gated by the exciting laser pulses and adjustable synchronization electronics. The minimal time gate was 5 ns. A frequency-doubled Q-switched Nd:YAG laser (pulse duration, 2 ns; repetition frequency, 10 Hz) or a tunable dye laser pumped by the third harmonic of the Nd:YAG laser was used as the excitation source. Fluorescence spectra and images were integrated over 10 s. Additional time-integrated (cw) measurements were carried out by using the 546-nm band of a high-pressure mercury lamp.

We measured the *in vivo* fluorescence of human skin including a small area of Er:YAG- and ALA-treated skin [85]. A time gate of 5 ns was chosen and the time delay was varied. The autofluorescence spectrum in the detection range 0–5 ns consists of a superposition of the strong emission (with a maximum in the green) due to endogenous fluorophores, such as coenzymes, collagen, and elastin, and the ALA-induced porphyrin fluorescence. The PP IX peak at 635 nm becomes prominent for increasing time delays (Fig. 20). Figure 21 shows the time-integrated image (Fig. 21a) and the time-gated image in the range of 20–45 ns (Fig. 21b). The first one shows a strong autofluorescence from the whole illuminated skin area, whereas the time-gated one indicates the smaller spot of PP IX emission.

In situ time-gated images were also obtained from the teeth of people, with the aim of detecting caries and dental plaque. For that purpose the ultrafast-shutter camera was equipped with a zoom camera objective. The teeth were irradiated by means of a single fiber transmitting the pulsed laser light. The time-integrated image (detection range, 590–800 nm) shows a nearly homogeneously distributed fluorescence over the whole tooth. This image is determined mainly by the autofluorescence, which has its maximum in the short-wavelength spectral region (Fig. 22a). However, with an appropriate time delay of more than 10 ns (here: detection time, 30–55 ns), only caries and plaque regions become obvious (Fig. 22b). As mentioned before, these regions contain bacteria which produce mainly PP IX.

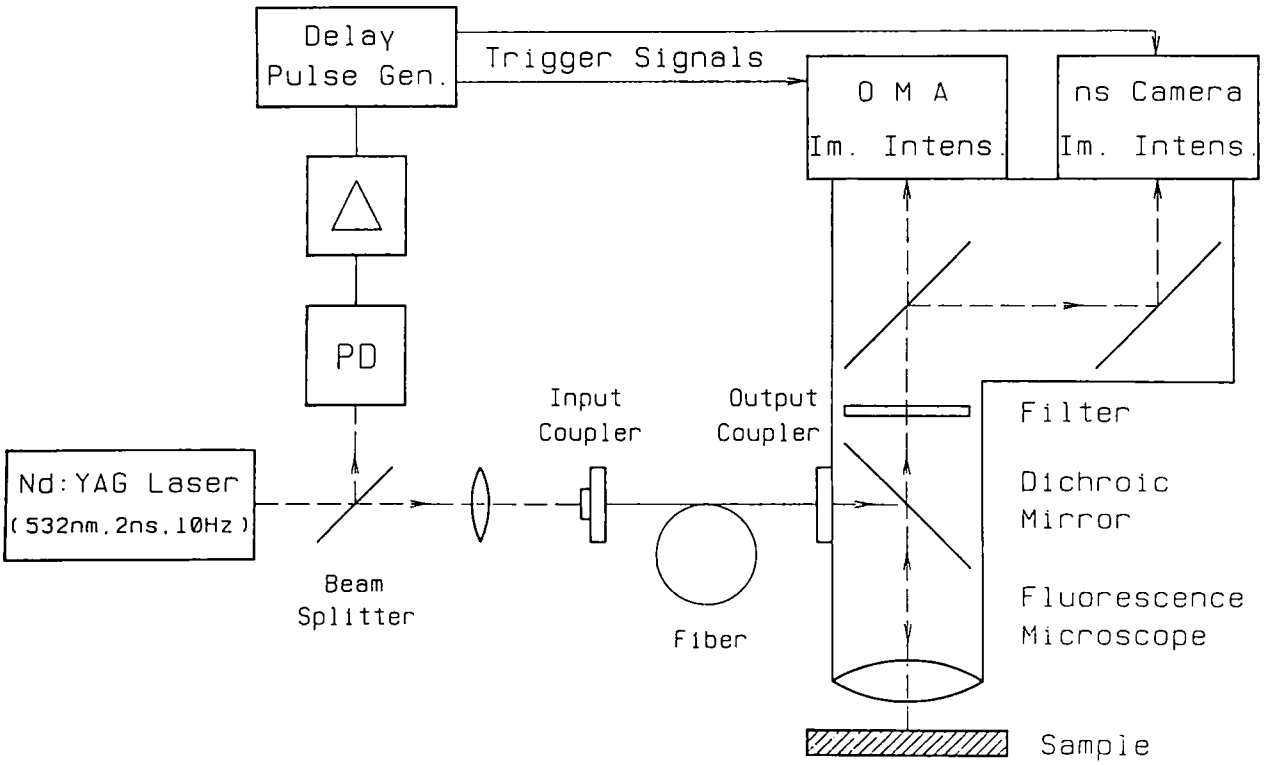

Fig. 19. Experimental setup for time-gated measurements.

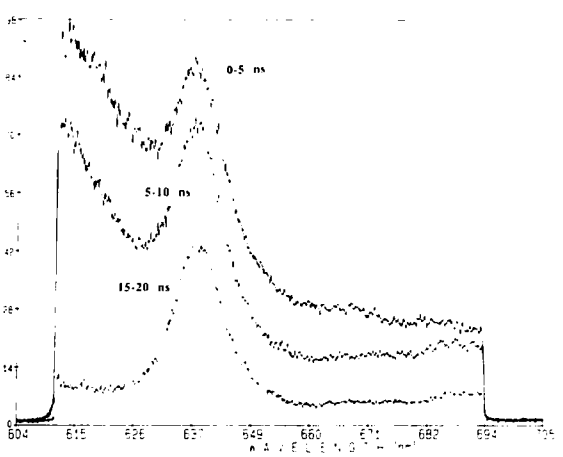

Fig. 20. Time-gated fluorescence spectra of ALA-treated skin.

AUTOFLUORESCENCE MODIFICATIONS DURING PHOTOTHERAPY

The porphyrin fluorophores, in particular PP IX, act as highly efficient photosensitizers. Irradiation results in the population of the first singlet state ^1P. This electronic state serves as the initial state for fluorescence emission and also for the transition into the triplet state by intersystem crossing (ISC). Metal-free porphyrins possess an ISC rate of up to 0.9 [99]. Porphyrins in the long-lived triplet state ^3P can transfer energy to molecular oxygen, which results in the formation of singlet oxygen. The process is called type II photooxidation [27].

$$^0P \xrightarrow{hf} {}^1P$$

$$^1P \xrightarrow{ISC} {}^3P$$

$$^3P + O_2 \xrightarrow{\text{energy transfer}} {}^0P + {}^1O_2$$

In addition, type 1 photooxidation occurs when ^3P participates in charge transfer reactions which lead to the formation of highly reactive radicals. Singlet oxygen and oxygen radicals cause cytotoxic reactions which can be used for photodynamic therapy (PDT), especially for the treatment of cancer [27]. A substantial portion of clinical PDT is currently based on the use of the photosensitizer HPD, a mixture of different por-

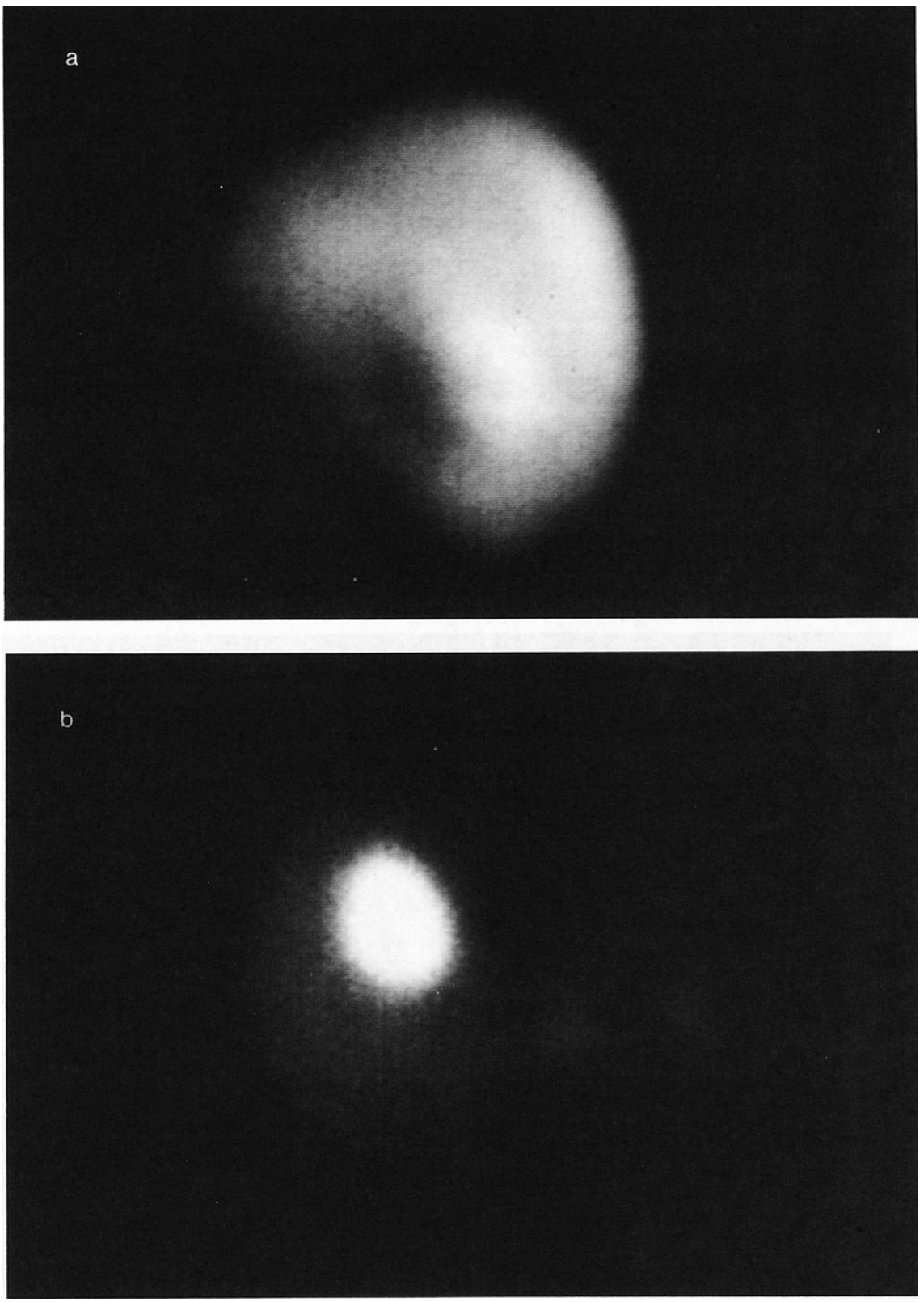

Fig. 21. Time-gated *in vivo* fluorescence images of human skin. The stratum corneum was removed by an Er:YAG laser, allowing penetration of ALA in the epidermis. (a) The time-integrated (cw-excitation) image (image size, 2.5 × 3 mm²) of the treated and surrounding unaffected skin. The whole illuminated skin area fluoresces. (b) In contrast, the time-gated image (detection range: 390–800 nm, 20–45 ns) shows a smaller fluorescent area due to PP IX fluorescence.

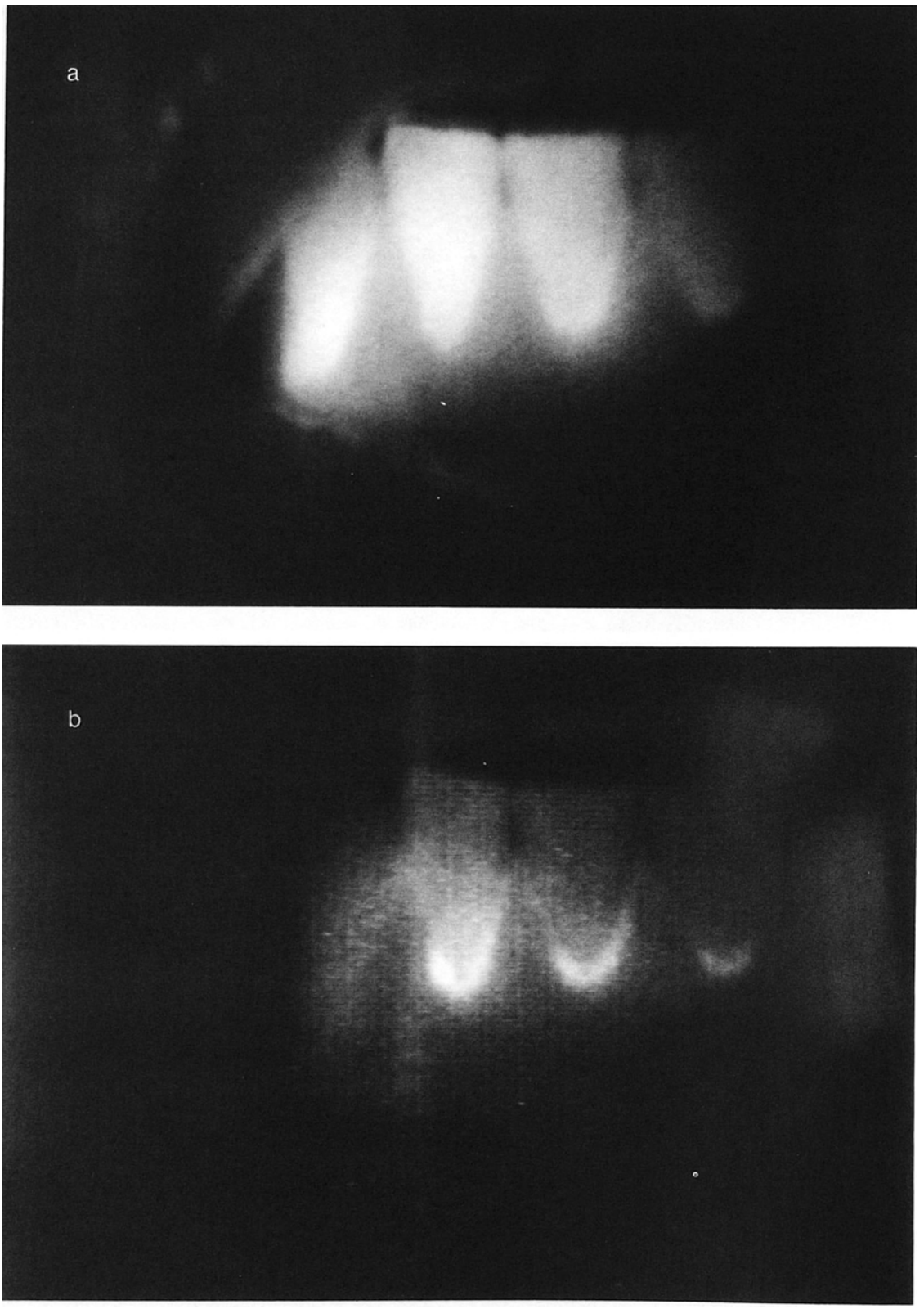

Fig. 22. *In vivo* fluorescence video images of the teeth of a proband using time-integrated (a) and time-gated (b) (30- to 55-ns) detection. Carious regions and dental plaque become obvious in the time-gated video images.

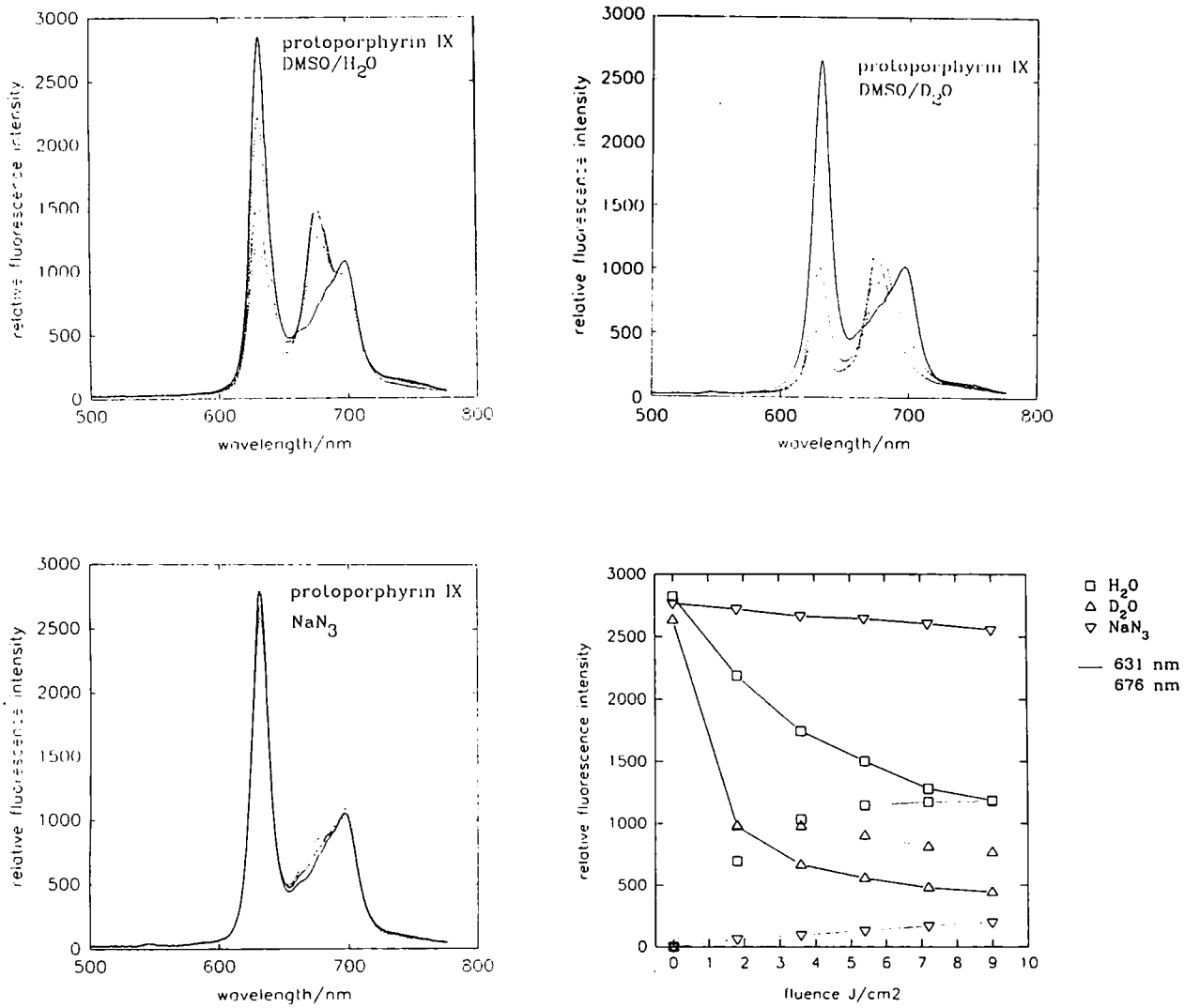

Fig. 23. Singlet oxygen-dependent photoproduct formation. The lifetime of singlet oxygen is 10-fold higher in D_2O compared with H_2O. NaN_3 is a well-known singlet oxygen quencher.

phyrins. A novel, successful approach to PDT using ALA-induced PP IX as photosensitizer has also been described [28].

The above photophysical scheme suggests that the porphyrin molecule should revert to the ground-state ^0P after the final energy transfer step. However, destruction processes occur which result in sensitizer photobleaching and in the formation of fluorescent photoproducts [97,100–103]. The chlorin-type photoproducts of PP IX fluoresce at 670 nm. They have fluorescence decay times of about 1 and 5 ns. We found that singlet oxygen is involved in the conversion of PP IX into photoproducts (Fig. 23). Therefore, on-line measurements of ALA-stimulated autofluorescence during PDT can give information on the formation of singlet oxygen and, thus, on the efficiency of a treatment.

Figure 24 demonstrates the photoinduced modifications to the ALA-induced PP IX autofluorescence during PDT of tumor-bearing nude mice [103]. Note the decrease in fluorescence at 635 and 710 nm due to photobleaching and the increase at 670 nm due to photoproduct formation. Further irradiation resulted in a slow decrease in the 670-nm emission at a lower bleaching rate than the original 635-nm fluorescence. Similar results were found during the PDT of patients with psoriasis and topical ALA administration (Fig. 25) or during

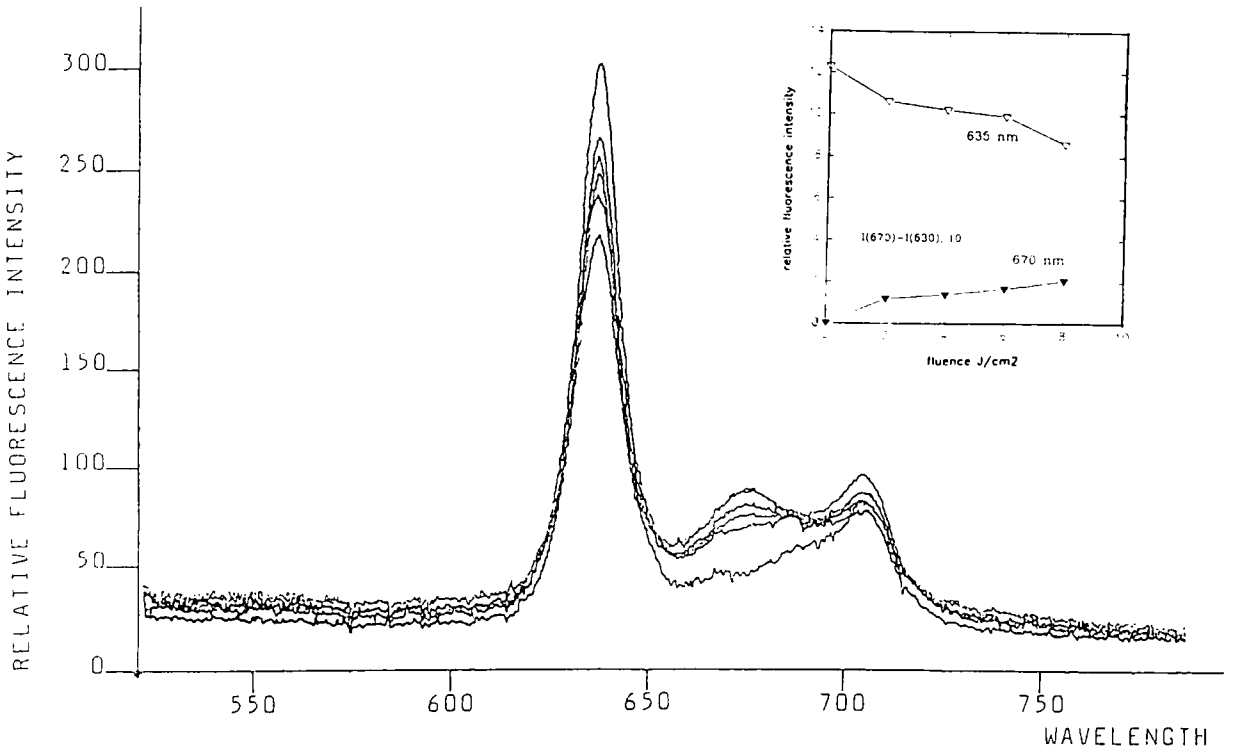

Fig. 24. Photoinduced modifications of the ALA-induced tumor autofluorescence during PDT. Note the fluorescence increase at 670 nnm.

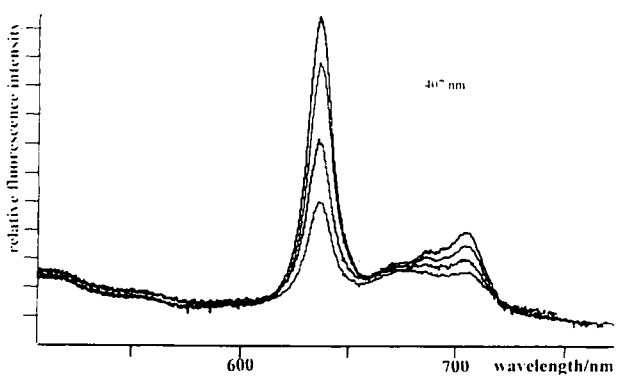

Fig. 25. Modifications of the ALA-stimulated autofluorescence of psoriasis during PDT.

the irradiation of nonincubated bacterial cultures of *P. acnes* [65].

Fluorescence decay curves of the *in vivo* tumor fluorescence before and after irradiation are depicted in Fig. 26. The nonirradiated tumor shows a slow decay, with a main fluorescence lifetime of about 17 ns. Irradiation results in a decrease in the integrated fluorescence and a shortening of the decay times to values typical for photoproducts.

These results indicate that spectral analysis and time-resolved/time-gated fluorescence measurements are appropriate tools for the detection of photoinduced destruction of photodynamically active endogenous porphyrins. Further investigations are necessary to correlate fluorescence modifications with PDT efficiency.

CONCLUSION

Autofluorescence of cells and tissues yields information on a broad variety of processes, including the metabolic function of the respiratory chain, the status of redox systems, the existence of various microorganisms, the involvement of bacteria in disease, and the existence of malignant cells.

Autofluorescence in the blue/green spectral region seems to be an appropriate tool for the determination of oxygen consumption and cell and tissue vitality and the detection of diseases associated with mitochondrial deficiencies or rapid cell growth. Fluorescence in the red is based mainly on endogenous porphyrins and can arise from defects in heme synthesis or microorganism activity. Bacteria-involved diseases, such as acne vulgaris, otitis externa, dental caries, and plaque, can therefore

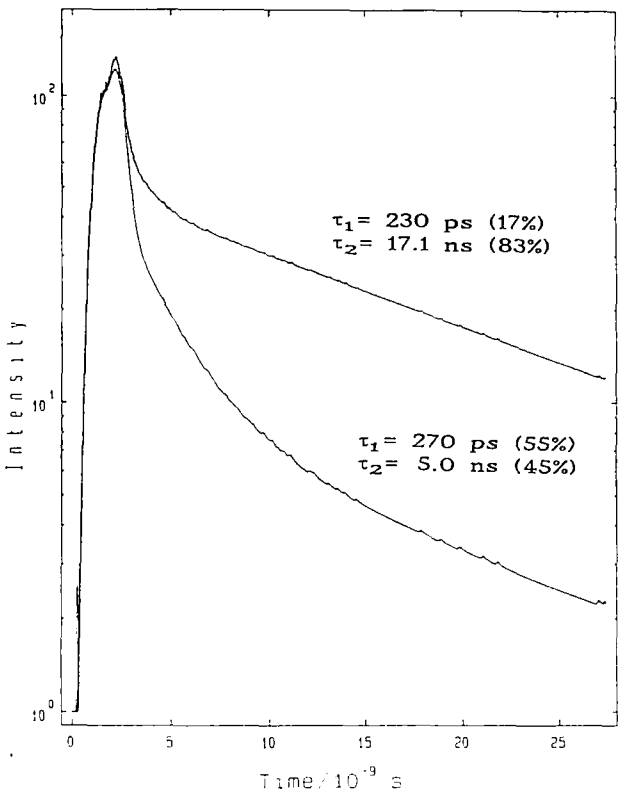

Fig. 26. Fluorescence decay kinetics of the ALA-induced tumor fluorescence before and after irradiation. The shortening of the decay times can be explained by the formation of short-lived photoproducts.

be detected. In addition, phototreatment based on the photodynamic activity of porphyrin fluorophores seems to be possible, particularly when the biosynthesis of the photodynamically active fluorophore PP IX is stimulated.

Time-gated measurements allow the detection of individual intrinsic fluorophores on the basis of their decay times. In particular, high-contrast fluorescence images of monomeric PP IX offers new detection possibilities. For example, we have shown that "caries images" and "dental plaque images" can be obtained and stored on normal videotape.

Interestingly, endogenous porphyrins undergo metallation processes (insertion of zinc or iron) and photoinduced destruction processes (transition into reduced porphyrins) resulting in modifications of their autofluorescence. Detection of photoinduced fluorescence changes can be used to yield information on photodynamically generated singlet oxygen and on the efficiency of porphyrin-based PDT. Therefore, *in situ* autofluorescence measurements may assist clinicians during an ALA-based photodynamic therapy.

ACKNOWLEDGMENTS

This work was performed with support from the Deutsche Forschungsgemeinschaft (DFG grant) and NIG Project 5P41 RR01192. The authors thank Bruce Tromberg and Sol Kimel for their outstanding contribution.

REFERENCES

1. D. Creed (1984) *Photochem. Photobiol.* **39,** 537–562.
2. D. Creed (1984) *Photochem. Photobiol.* **39,** 563–575.
3. A. White *et al.* (1978) *Principles of Biochemistry,* McGraw-Hill, New York.
4. National Academy of Sciences (1984) *Specifications and Criteria of Biochemical Compounds,* 3rd ed., Sigma Chemical Company, St. Louis, MO.
5. J. Lakowicz (1986) *Principles of Fluorescence Spectroscopy,* Plenum Press, New York.
6. S. D. Kozikowski, L. J. Wolfram, and R. R. Alfano (1984) *IEEE-QE* **12,** 1379–1382.
7. J. H. Aiken and C. W. Hui (1991) *Anal. Lett.* **24,** 167–180.
8. R. R. Alfano *et al.* (1984) *IEEE-QE* **20,** 1507–1511.
9. A. R. Holzwarth and T. A. Roelofs (1992) *J. Photochem. Photobiol. B* **15,** 45–62.
10. H. Schneckenburger and W. Schmidt (1992) *J. Photochem. Photobiol. B* **13,** 190–193.
11. C. Lee (1974) *Biochem. Biophys. Res. Commun.* **60,** 838–843.
12. J. M. Salmon *et al.* (1982) *Photochem. Photobiol.* **36,** 585–593.
13. P. Galland and H. Senger (1988) *J. Photochem. Photobiol. B* **1,** 277–294.
14. M. Sun, T. A. Moore, and P. S. Song (1972) *J. Am. Chem. Soc.* **94,** 1730–1740.
15. K. Koenig *et al.* (1994) In W. Waidelich (Ed.), *Laser. Optoelectronics in Medicine* (in press).
16. H. Schneckenburger and K. Koenig (1992) *Opt. Eng.* **31,** 1447–1451.
17. B. Chance *et al.* (1962) *Science* **137,** 499–508.
18. B. Chance and F. F. Josis (1959) *Nature* **184,** 195–196.
19. C. Y. Guezennec *et al.* (1991) *Eur. J. Appl. Physiol.* **63,** 36.
20. A. Mayevski (1984) *Brain Res. Rev.* **7,** 49–68.
21. W. Lohmann and E. Paul (1988) *Naturwissenschaften* **75,** 201–202.
22. W. Lohmann *et al.* (1990) *Z. Naturforsch.* **45c,** 1063–1066.
23. H. Schneckenburger, A. Rueck, and O. Haferkamp (1989) *Anal. Chim. Acta* **227,** 227–233.
24. H. Schneckenburger, P. Gessler, and I. Pavenstaedt-Grupp (1992) *J. Histchem. Cytochem.* **40,** 1573–1578.
25. P. S. Song (1980) in H. Senger (Ed.), *The Blue Light Syndrome,* Springer, Berlin, pp. 157–171.
26. K. Koenig *et al.* (1994) *SPIE Budapest* **2086** (in press).
27. D. R. Doiron and O. J. Gomer (1983) *Porphyrin Localization and Treatment of Tumours,* Alan R Liss, New York.
28. J. C. Kennedy and R. H. Pottier (1992) *J. Photochem. Photobiol. B* **14,** 275–292.
29. A. K. Gupta and T. F. Anderson (1987) *J. Am. Acad. Dermatol.* **17,** 703–734.
30. J. W. Young and E. T. Conte (1991) *Int. J. Dermatol.* **30,** 399–404.
31. D. Fuchs *et al.* (1990) *AIDS* **4,** 341–344.
32. H. N. Shah *et al.* (1979) *Biochem. J.* **180,** 45–50.
33. C. E. Cornelius and G. D. Ludwig (1967) *J. Invest. Derm.* **49,** 368–370.
34. B. Kjeldstad, A. Johnsson, and S. Sandberg (1984) *Arch. Dermatol. Res.* **276,** 396–400.

35. A. Johnsson, B. Kjeldstad, and T. B. Melo (1987) *Arch. Dermatol. Res.* **279,** 190–193.
36. J. S. Brazier (1986) *J. Appl. Bacteriol.* **60,** 121–126.
37. R. L. Harms, D. R. Martinez, and V. M. Griego (1986) *Appl. Environ. Microbiol.* **51,** 481–486.
38. R. de la Fuente *et al.* (1986) *FEMS Microbiol Lett.* **35,** 183–188.
39. K. Koenig, W. Dietel, and H. Schubert (1989) *Neoplasma* **36,** 135–138.
40. G. Weagle *et al.* (1988) *J. Photochem. Photobiol. B* **2,** 313–320.
41. K. Koenig *et al.* (1994) *SPIE Budapest* **2078** (in press).
42. B. A. Tapper *et al.* (1975) *J. Sci. Food Agr.* **26,** 277–284.
43. A. Policard (1924) *C.R. Soc. Biol.* **91,** 1423–1424.
44. S. Bommer (1927) *Klin. Wochenschr.* **24,** 1142–1144.
45. H. Gougerot and A. Patte (1939) *Bull. Soc. Franc. Derm. Syph.* **46,** 288–295.
46. F. Rochese (1954) *Oral Surg. Oral Med. Oral Pathol.* **7,** 353–362.
47. D. Sharvill (1955) *Trans. St. John's Hosp. Derm. Soc. (London)* **34,** 32–36.
48. F. N. Ghadially (1960) *J. Pathol. Bact.* **80,** 345–361.
49. F. N. Ghadially and W. J. P. Neish (1960) *Nature* **188,** 1124.
50. F. N. Ghadially, W. J. P. Neish, and H. C. Dawkins (1963) *J. Pathol. Bact.* **85,** 77–92.
51. D. M. Harris and J. Werkhaven (1987) *Lasers Surg. Med.* **7,** 467–472.
52. Y. Yuanlong *et al.* (1987) *Lasers Surg. Med.* **7,** 528–532.
53. W. Dietel, K. Koenig, and P. Dorn (1988) *Laser-Induced Autofluorescence of Tumors,* PDT School, Berlin.
54. K. Koenig, J. Hemmer, and H. Schneckenburger (1992) in P. Spinelli, M. DalFante, and R. Marchesini (Eds.), *Photodynamic Therapy and Biomedical Lasers,* Elsevier, Amsterdam, pp. 903–906.
55. R. Margalit and S. Cohnes (1985) *J. Inorg. Biochem.* **25,** 187–195.
56. S. Sommer, C. Rimington, and J. Moan (1984) *FEBS* **172,** 267–271.
57. S. Montan and L. G. Stroemblad (1987) *Lasers Life Sci.* **1,** 275–285.
58. J. Hung *et al.* (1991) *Lasers Surg. Med.* **11,** 99–105.
59. G. C. Tang and R. R. Alfano (1989) *Lasers Surg. Med.* **9,** 290–295.
60. S. Svanberg *et al.* (1994) *SPIE Budapest* **2081** (in press).
61. I. Formanek *et al.* (1977) *Arch. Dermatol. Res.* **259,** 169–176.
62. D. Fanta *et al.* (1981) *Arch. Dermatol. Res.* **271,** 127–133.
63. D. Fanta *et al.* (1978) *Arch. Dermatol. Res.* **261,** 175–179.
64. W. S. Lee, A. R. Shalita, and M. B. Poh-Fitzpatrick (1978) *J. Bacteriol.* **133,** 811–815.
65. K. Koenig, A. Rueck, and H. Schneckenburger (1992) *Opt. Eng.* **31,** 1470–1474.
66. H. Meffert. Personal communication.
67. A. V. Lassus *et al.* (1983) *Dermatol. Monatsschr.* **169,** 376–379.
68. H. C. Benedict (1928) *Science* **67,** 442.
69. R. L. Hartles and A. G. Leaver (1953) *Biochem. J.* **54,** 632–638.
70. W. G. Armstrong (1963) *Arch. Oral Biol.* **8,** 79–90.
71. R. R. Alfano and S. S. Yao (1981) *J. Dent. Res.* **80,** 120–122.
72. H. Bjelkhagen (1981) *IEEE-QE* **17,** 226–228.
73. H. Bjelkhagen *et al.* (1982) *Swed. Dent. J.* **6,** 1–7.
74. R. R. Alfano *et al.* (1984) *IEEE-QE* **20,** 1512–1515.
75. S. Albin, C. E. Byvik, and A. M. Buonchristini (1988) *SPIE* **907,** 96–98.
76. U. Hafstoem-Bjoerkman *et al.* (1991) *Acta Odontol. Scand.* **49,** 27.
77. K. Koenig *et al.* (1993) *SPIE* **907,** 125–131.
78. K. Koenig *et al.* (1994) *SPIE Budapest* **2080** (in press).
79. J. M. Hardie and G. H. Bowden (1974) in F. A. Skinner and J. G. Carr (Eds.), *Microbial Flora of Man,* Academic Press, New York, p. 58.
80. J. M. Li *et al.* (1989) *J. Bacteriol.* **171,** 2547–2552.
81. I. Z. Ades (1990) *Int. J. Biochem.* **22,** 565–578.
82. J. Z. Yang *et al.* (1993) *Photochem. Photobiol.* **57,** 803–807.
83. Z. Malik and M. Djaldetti (1979) *Cell. Different.* **8,** 223–233.
84. R. Baumgaertner *et al.* (1994) *SPIE Budapest* (in press).
85. H. Schneckenburger *et al.* (1994) *Opt. Eng.* (in press).
86. K. Koenig, F. Genze, and K. Miller (1993) *Dermatol. Monatsschr.* **179,** 132–134.
87. F. DeMatteis and B. E. Prior (1962) *Biochem. J.* **83,** 1–8.
88. F. DeMatteis and C. Remmington (1963) *Br. J. Dermatol.* **75,** 91–104.
89. A. M. Brady and E. A. Lock (1992) *Arch. Toxicol.* **66,** 175–181.
90. Z. Malik *et al.* (1994) *SPIE Budapest* **2078** (in press).
91. G. T. Javor and E. F. Febre (1992) *J. Bacteriol.* **174,** 1072–1075.
92. M. Doss and W. K. P. Dormston (1971) *Hoppe-Seyler Physiol. Chem.* **352,** 725–733.
93. W. K. Philipp-Dormston and M. Doss (1975) Overproduction of porphyrins and heme in heterotrophic bacteria. *Z. Naturforsch.* **30,** 425–426.
94. A. Andreoni *et al.* (1982) *Chem. Phys. Lett.* **88,** 33–36.
95. M. Yamashita *et al.* (1984) *IEEE-QE* **20,** 1363–1369.
96. H. Schneckenburger, H. K. Seidlitz, and J. Eberz (1988) *J. Photochem. Photobiol. B* **2,** 1–19.
97. K. Koenig, H. Wabnitz, and W. Dietel (1990) *J. Photochem. Photobiol. B* **8,** 103–111.
98. H. Schneckenburger *et al.* (1994) in W. Waidelich (Ed.), *Laser '93—Optoelectronics in Medicine,* Springer, Berlin–Heidelberg (in press).
99. R. Pottier and T. G. Truscott (1986) *Int. J. Radiat. Biol.* **50,** 421–452.
100. P. Valat, G. D. Reinhardt, and D. M. Jameson (1988) *Photochem. Photobiol.* **47,** 787–790.
101. W. Dietel, K. Koenig, and E. Zenkevich (1990) *Lasers Life Sci.* **3,** 197–203.
102. H. K. Seidlitz *et al.* (1992) *Opt. Eng.* **31,** 1482–1486.
103. K. Koenig *et al.* (1993) *J. Photochem. Photobiol. B* **18,** 287–290.